Published in final edited form as:
J Cell Physiol. 2011 December ; 226(12): 3132–3146. doi:10.1002/jcp.22669.

The suppression of myosin light chain (MLC) phosphorylation during the response to lipopolysaccharide (LPS): beneficial or detrimental to endothelial barrier?

Natalia V. Bogatcheva[1,*], **Marina A. Zemskova**[1], **Christophe Poirier**[1], **Tamara Mirzapoiazova**[2], **Irina Kolosova**[3], **Anne R. Bresnick**[4], and **Alexander D. Verin**[1]

[1]Vascular Biology Center, Medical College of Georgia, Augusta, GA 30912

[2]Dept of Medicine, University of Chicago, Chicago, IL, 60637

[3]Dept of Anesthesiology, Johns Hopkins University, Baltimore, MD 21205

[4]Dept of Biochemistry, Albert Einstein College of Medicine, Bronx, NY 10461

Abstract

Sepsis-induced vascular leakage is a major underlying cause of the respiratory dysfunction seen in severe sepsis. Here we studied the role of MLC phosphorylation in LPS-induced endothelial hyperpermeability and assessed how the changes in phospho-MLC distribution affect LPS-induced barrier dysfunction. We demonstrated that the changes in human lung microvascular endothelial permeability are preceded by the increase in intracellular calcium level, and increase in MYPT and MLC phosphorylation. Using the siRNA approach, we showed that both LPS-induced barrier dysfunction and MLC phosphorylation are attenuated by the depletion of the smooth muscle isoform of MLC kinase (MLCK) and Rho kinase ROCK2. Surprisingly, pharmacological inhibition of both ROCK1 and 2 with Y-27632 exacerbated LPS-induced drop in transendothelial resistance, although significantly decreasing MLC phosphorylation level. We next studied the involvement of protein kinase A (PKA)-dependent pathways in LPS-induced barrier dysfunction. We showed that LPS decreased the level of PKA-dependent phosphorylation in endothelial cells; and the pretreatment with forskolin or PKA activator bnz-cAMP counteracted this effect. Forskolin and bnz-cAMP also attenuated LPS-induced increase in MLC phosphorylation level. As we have shown earlier (Bogatcheva et al., 2009), forskolin and bnz-cAMP provide protection from LPS-induced barrier dysfunction. We compared the effects of bnz-cAMP and Y-27632 on phospho-MLC distribution and observed that while bnz-cAMP increased the association of the phospho-MLC signal with the cortical structures, Y-27632 decreased this association. These data indicate that an overall decrease in MLC phosphorylation could be either beneficial or detrimental to endothelial barrier, depending on the intracellular locale of major phospho-MLC changes.

Keywords

MLCK; ROCK; PKA; LPS; MLC phosphorylation

Gram-negative bacterial wall component LPS (endotoxin) is routinely used to mimic gram-negative sepsis and to study the mechanisms of sepsis complications such as Acute Lung Injury (ALI) and Adult Respiratory Distress Syndrome (ARDS) (Jacobson and Garcia, 2007; Opal, 2007). Despite the current advances in the treatment of sepsis, severe sepsis is

[*]Correspondence to: Natalia V. Bogatcheva, Medical College of Georgia, 1459 Laney Walker Blvd, CB-3701, Augusta, GA, 30912, Tel 706 721 1522, Fax 706 721 1536, nbogatcheva@mcg.edu.

still associated with high mortality rates (Martin et al., 2003). It is argued that respiratory dysfunction related to sepsis has a mortality impact independent of simultaneous non-pulmonary complications such as multiple organ failure (Martin and Bernard, 2002)

Experimental and clinical studies have suggested that dramatic impairment of gas exchange seen in sepsis is a direct consequence of the loss of endothelial and epithelial barrier functions resulting in lung edema and fluid accumulation in the alveolar space (Ware and Matthay, 2000). Regulation of barrier function is a complex process involving a variety of cytoskeletal and regulatory constituents which control two major routes, paracellular and transcellular (Komarova and Malik, 2010). Unlike vesicular-mediated transcellular route, the more widely studied paracellular route depends on the formation of gaps in the formerly intact endothelial monolayer. The current paradigm states that the increase in paracellular endothelial permeability is driven, on one hand, by the generation of the centripetal contractile forces and, on another, by the loss of junctional integrity, provided mostly by the tight and adherence junctions (Bogatcheva and Verin, 2008).

Both endothelial contractility and the maintenance of junctional organization depend on actomyosin filaments; however, whereas barrier-disruptive contractility involves the formation of cell-crossing stress fibers, barrier-maintaining intercellular junctions require strong anchorage to the cortical actomyosin structures. The state of actomyosin in endothelium is controlled by MLC phosphorylation, as the increased level of phospho-MLC is necessary to induce filament formation and to activate actomyosin ATPase (Goeckeler and Wysolmerski, 1995). The level of phospho-MLC, regulated by phosphorylation and dephosphorylation, mainly depends on the activity of two enzymes, MLC kinase (MLCK) and Rho kinase (ROCK). Both of them can directly phosphorylate MLC in vitro and in vivo (Fukata et al., 2001; Kamm and Stull, 2001). At the same time, ROCK-mediated inactivation of myosin phosphatase also serves to increase MLC phosphorylation level (Matsumura and Hartshorne, 2008). Both MLCK and ROCK-dependent pathways could be modulated by the activity of protein kinase A (PKA), known to decrease MLC phosphorylation level (Lorenowicz et al., 2007).

In this manuscript, we aimed to analyze the particular involvement of MLC phosphorylation process in LPS-induced barrier dysfunction. Over the years, the use of pharmacological inhibitors, specific siRNAs or genetically modified animals allowed us to better understand the role of enzymes controlling MLC phosphorylation in lung edema development. MLCK involvement was shown in LPS-induced epithelial and endothelial hyperpermeability (Eutamene et al., 2005; Mirzapoiazova et al.; Moriez et al., 2005; Wainwright et al., 2003); however, the existence of several MLCK isoforms originating from the same gene (Garcia et al., 1997; Verin et al., 1998b) complicated the analysis of the roles of individual isoforms.

ROCK involvement in the regulation of endothelial permeability, although seemingly obvious (Essler et al., 2000), also posed certain questions. ROCK depletion with specific siRNA showed that the effects of individual isoforms knock-downs on MLC phosphorylation can be dissociated from their effects on permeability (Mong and Wang, 2009). Temporal dissociation of Rho/ROCK activation from the onset of LPS-induced hyperpermeability in dermal endothelium (Schlegel et al., 2009) only strengthened this hypotheses. Application of Y-27632 in animal models of LPS-induced injury rendered disparate results (Lundblad et al., 2004; Tasaka et al., 2005). Altogether, these data failed to deliver a clear perspective of the ROCK involvement in LPS-induced barrier dysfunction, raising the possibility that ROCK impact can be both species- and endothelium-specific. Therefore, the analysis of ROCK1/2 contribution to human lung endothelial hyperpermeability was necessary to evaluate the therapeutic potential of the pharmacological inhibition of this pathway. This analysis would complement the analysis of

MLCK involvement and let us assess the role of MLC phosphorylation in the response to LPS more clearly.

Earlier we have shown that an increase of intracellular cAMP and subsequent PKA activation counteracts LPS-induced barrier dysfunction in HLMVEC (Bogatcheva et al., 2009). The downstream pathways linking cAMP elevation to barrier-protective cytoskeletal rearrangements are numerous and involve cAMP effectors PKA and RAP1 guanidine exchange factor Epac1 (Lorenowicz et al., 2007). Epac1 involvement in barrier enhancement was strongly linked to the regulation of the state of adherence junctions (Kooistra et al., 2005). PKA down-stream pathways include phosphorylation of VASP (Comerford et al., 2002), down-regulation of Rho/ROCK pathway (Qiao et al., 2003), direct inactivation of MLCK (Nishikawa et al., 1984) or activation of protein phosphatase1 activity toward myosin (Bindewald et al., 2004). As several PKA-mediated pathways converge on the regulation of MLC phosphorylation level, the analysis of PKA-dependent suppression of LPS-induced MLC phosphorylation could help us gain additional information about the role of MLC phosphorylation in the regulation of barrier function.

The first objective of the present study was to determine whether knockdown/inhibition of the individual isoforms of MLCK and ROCK would have an effect on LPS-induced hyperpermeability of the lung microvascular endothelium. The second objective was to elucidate the mechanism linking PKA-induced alteration of MLC phosphorylation level to the alleviation of LPS-induced barrier dysfunction. Comparison of the effects of pharmacological MLCK and ROCK inhibition to the effect of siRNA-mediated knockdowns demonstrated certain limitation of the pharmacological approach. siRNA studies revealed the critical involvement of smooth muscle MLCK and ROCK2 in LPS-induced MLC phosphorylation and barrier dysfunction. We next compared the effect of barrier-protective agents forskolin and bnz-cAMP (Bogatcheva et al., 2009) against the effect of Y-27632, which in our study was shown to be barrier-disruptive. Although both types of agents reduced MLC phosphorylation, the analysis of the intracellular distribution of phospho-MLC signal allowed us to gain certain insights on how the balance between the cortical phospho-MLC signal and the stress fiber-originated phospho-MLC signal affects the barrier in the presence of LPS.

Materials and Methods

Reagents

LPS from *E.coli* (0127:B8, with activity of 900 000 u/mg) and forskolin were purchased from Sigma. Calcium chelator BAPTA-AM, inhibitors ML7, Y-27632 and GSK429286 were from Calbiochem (La Jolla, CA). N^6-benzoyl-cAMP (bnz-cAMP) and 8-(4-chlorophenythio)-2'-O-methyl-cAMP (o-me-cAMP) were from Biolog Life Science Institute (Bremen, Germany). MLC, diphospho-MLC and PKA phosphorylation site-specific antibodies were from Cell Signaling (Beverly, MA). Myosin phosphatase regulatory subunit (MYPT1) and phospho-MYPT Ser696 antibodies were from Millipore (Billerica, MA). ROCK1 and 2 antibodies were from BD biosciences (San Jose, CA). Beta-actin antibody was from Sigma (St. Louis, MO). GAPDH antibody was from Abcam (Cambridge, MA). Reagents used for immunofluorescent staining were obtained from Invitrogen (Carlsbad, CA). ROCK1-specific siRNA was from Qiagen (Valencia, CA). MLCK and ROCK2-specific siRNAs were from Santa Cruz. Non-specific control siRNA-1 was from Ambion (Austin, TX).

Cell culture

Human lung microvascular endothelial cells (HLMVEC) were purchased from Lonza (Walkersville, MD) and used at the passages 6–7. They were cultured in media containing 5% FBS and maintained at 37°C in a humidified atmosphere of 5%CO_2–95% air. Primary culture of human umbilical vein endothelial cells (HUVEC) was provided by Dr. J. Catravas laboratory (Medical College of Georgia, Augusta, GA). The confluence of monolayers was assessed using phase contrast microscopy. Monolayers were considered over-confluent when existed in culture 2–3 days after reaching the confluence.

Measurement of transendothelial permeability

Transendothelial electrical resistance (TER) was measured using the highly sensitive biophysical assay with an electrical cell-substrate impedance sensor (Applied biophysics, Troy, NY) as described previously (Verin et al., 2001). HLMVEC monolayers were considered confluent when they reach the resistance of 2000 Ohm. Transendothelial permeability for macromolecular tracers was measured with Chemicon/Millipore (Billerica, MA) in vitro vascular permeability assay utilizing 2000 kDa FITC-Dextran. For both assays, media was changed to the fresh complete media 1 hour prior the experiment.

Western immunoblotting

Cells were grown in 12-well or 6-well plates; media was changed to the fresh complete media 1 hour prior the experiment. After stimulation, cells were rinsed with ice-cold PBS and lysed with PBS containing 1% SDS and 20mM NaF. After freezing-thawing and aspiration through 25g needle, samples were supplemented with Western blot loading buffer and boiled. Protein extracts were separated on 4–20% gradient gels and transferred to nitrocellulose membrane. After staining with specific antibodies, enhanced chemiluminescent signal was visualized directly using Image Station 440 from Kodak. The images were quantitated with Kodak MI imaging software. The intensity of the specific bands was normalized to the intensity of GAPDH or β-actin bands.

Measurement of intracellular calcium level

Intracellular calcium level was assessed using Fluo-4 Direct Calcium assay kit (Invitrogen) according to the manufacturer instruction. Briefly, HLMVEC grown to confluence in the wells of 96-well plate were pre-loaded with Fluo-4 for 4h. Basal fluorescence of quiescent cells was monitored for 5 min using Titertek Fluoroscan II plate reader. Cells were challenged with LPS and vehicle control; changing fluorescence was monitored repeatedly to assess the response. Basal fluorescence value was subtracted from the values obtained after the challenge.

Depletion of endogenous MLCK, ROCK1 and ROCK2 in EC

To reduce the expression of endogenous proteins, HLMVEC plated in plates (with or without coverslips) or in ECIS chambers were treated with 50 nM siRNA of specific siRNA, non-specific non-silencing siRNA, or DharmaFECT1 transfection reagent (Dharmacon Research, Lafayette, CO). Transfection was performed according to manufacturer instructions in monolayers grown to ~70% confluence. Cells were used for the described above experiments 48 h post-transfection.

RT-PCR

RNA extracted with trizol (Invitrogen, Carlsbad, CA) was subjected to standard reverse transcription reaction with RT-MMLV reverse transcriptase (Promega, Madison, WI). All the primers except F3/R3 were designed with the on-line Primer3 software (http://fokker.wi.mit.edu/primer3/input.htm) and purchased from Eurofins MWG Operon

(Huntsville, AL). Non-muscle MLCK/*MYLK*-specific F3/R3 primers were designed to amplify the PCR fragment described in the original report (Verin et al., 1998b): MYLK-F3 forward primer 5'-GCCTTTGGATCCAGGAAGTG-3'; MYLK-R3 reverse primer 5'-TCGTCCACCTCCTGCTGGCG-3' for the amplification of 646bp cDNA. Other primers specific for the non-muscle MLCK were: MYLK-F1 5'-CCTAGCTGAGAATGCCTTGG-3' and MYLK-R1 5'-TAGTGACCTGGCTTCCATCC-3' for the amplification of 176bp cDNA; MYLK-F4 5'-AGCTTGGTCAGCCTGTTGTT-3' and MYLK-R4 5'-CACGTGTACACTCCCACGTC-3' for the amplification of 310bp cDNA; MYLK-F5 5'-TTCAGCCTTGTGATTCATGC-3 ' and MYLK-R5 5'-CATGCCGTTCTTCTCAGACA-3' for the amplification of 381bp cDNA.

Primers common to non-muscle and smooth-muscle MLCK were: MYLK-F2 5'-CCCGTGCTAGGAACTGAGAG-3', MYLK-R2 5'-TTCTCGCTGTTCTCCACCTT-3' for the amplification of a 289bp cDNA.

Primers specific to telokin were: TELO-F 5'-TCAGGAGGTCCTTGTTCCAG-3', TELO-R 5'-TCAAGGAAAGCTTGGGACAC-3' for the amplification of a 289bp cDNA.

Primers specific for house-keeping gene *HPRT* were: HPRT-F 5'-AATCCAAAGATGGTCAAGGTC-3', HPRT-R 5'-GCGATGTCAATAGGACTCCAG-3' for the amplification of a 249bp cDNA.

Amplification of cDNA was performed with GoTaq DNA polymerase from Promega (Madison, WI) using PCR Sprint Thermal Cycler from Thermo Scientific (Waltham, MA); annealing temperature of 55°C.

Real time PCR

Comparative C_t method was used to assess the level of *MLCK/MYLK* mRNA (primers F2/R2) in cells pretreated with MLCK siRNA or cells treated with 100ng/ml LPS. The analysis of *MYLK* expression with *HPRT* expression endogenous control was done using Step-One Real-Time PCR system from Applied Biosystems (Foster City, CA). Amplification was monitored by incorporation of SYBR Green dye (Applied Biosystems) into the double strand cDNA.

Construction of MLC expression vectors, nucleofection and MLC detection

The wild-type and T18AS19A Xenopus myosin-II regulatory light chains (Bresnick et al., 1995) were sublconed into the *Sac*II/*Xba*I sites of pUHD10-3 vector (kindly provided by Dr. Hermann Bujard, University of Heidelberg). In this vector, the cDNA transcription is under control of tet-operators and requires the co-expression of tetracycline-controlled transactivator tTA. For both constructs, a Kozak consensus sequence was incorporated into the expression construct to render efficient translation. All constructs were confirmed by DNA sequencing.

HLMVEC were co-transfected with a mixture of MLC- and GFPmax-expressing constructs using Amaxa nucleofection technology (Lonza, Basel, Switzerland) according to manufacturer protocol. Cells plated in the chambers with the gold electrodes were allowed to attach for 24h, then infected with 20 moi AdCMVtTA (Eton Bioscience Inc, San Diego, CA). Media was supplemented with 2 μg/ml doxycycline to silence MLC expression when needed. 48h later, TER was analyzed and cells were collected for Western Blot analysis. The efficiency of transfection was checked by direct GFPmax fluorescence and by Western blot using anti-xenopus MLC antibody; the efficiency of infection was checked using anti-VP16 antibody.

Rabbit polyclonal antibodies to the Xenopus regulatory MLC (xMLC) were prepared using the full-length recombinant xMLC and standard methods. Briefly, New Zealand white rabbits were injected subcutaneously with the xMLC in complete Freund's adjuvant; subsequent to the initial inoculation rabbits were boosted with the xMLC in incomplete Freund's adjuvant. Rabbits were bled following first, second and third boost to check antibody titers; after the third boost, rabbits were bled weekly. xMLC antibodies were purified by affinity chromatography on xMLC-Sepharose column. The specificity of the xMLC antibodies was assessed by immunoblot analysis. The antibodies recognize human MLC with lesser affinity than xMLC.

EC imaging

For immunofluorescence experiments, EC monolayers were plated on gelatin-covered coverslips. Media was changed to the fresh complete media 1 hour prior the experiment. Before immunostaining, cells were briefly washed with phosphate-buffered saline (PBS) and fixed in PBS solution of 4% formaldehyde. After permeabilization with 0.25% Triton X-100 and blocking, cells were stained with anti-ppMLC antibodies and Alexa594-phalloidin. After mounting in anti-fade mounting media, the coverslips were viewed and photographed with Zeiss Axio Observer video imaging system using Zeiss Axiovision software. To assess the distribution of signal, we analyzed the signal intensity profile along the line which was drawn across an individual cell in the close vicinity of, but not overlapping with the nuclear region. For this analysis, the cells of approximately same size and shape were selected from 5 different microscopic fields. The signal intensity (max value equal 1) was plotted versus cell width, and profiles from 5 different cells were overlapped to show the variations in signal distribution. To assess the intensity of the cortical ppMLC signal, we analyzed the intensity of peaks corresponding to the peripheral ppMLC structures. The thickness of these structures was assessed as the peak width measured at ½ of peak height. The background intensity was estimated from the analysis of each individual profile and subtracted to render the “true value” of the individual peak height.

Statistical analysys

Results from several parallel experiments were pooled to perform statistical analysis with one-way ANOVA test (Origin8 software, OriginLab, Northampton, MA); results with $p<0.05$ were considered significantly different.

Results

LPS-induced compromise of barrier function is preceded by MLC phosphorylation

Earlier, we have demonstrated that LPS causes a marked increase of permeability for water and ions across microvascular endothelial monolayer (Bogatcheva et al., 2009; Kolosova et al., 2008). Here we compare the time course of the transendothelial electrical resistance (TER) decline to the time course of the increased FITC-dextran permeation and show that both measurements render gradual and delayed changes in response to LPS, with no significant alterations in the first hour following LPS addition. The responses develop over the course of the next several hours and achieve maximum 6 hours post-LPS addition (Fig. 1A, B). The analysis of the level of MLC phosphorylation shows that mono- and diphospho-MLC content increases only slightly during the first hour of exposure to LPS, reaching its maximum at 2–4h post-LPS addition (Fig. 1C). Our results demonstrate that an increase in MLC phosphorylation precedes the maximal changes in endothelial permeability.

We next analyzed the potential contribution of Rho kinase (ROCK) in the LPS-induced increase of MLC phosphorylation. We observed an increase in myosin-targeting phosphatase 1 subunit (MYPT) phosphorylation in LPS–challenged cells suggesting that the

induction of MLC phosphorylation is at least partially achieved via ROCK/MYPT-dependent inactivation of myosin phosphatase (Fig. 1C). Earlier, the LPS-induced increase of MLC phosphorylation was shown to occur secondary to protein synthesis (Essler et al., 2000). Indeed, dramatic overexpression of the ROCK/MYPT cascade elements was seen in LPS-stimulated mesenteric arteries (da Silva-Santos et al., 2009). To check if LPS induces changes in the regulatory protein expression in HLMVEC, we assessed protein levels of ROCKs, MYPT, and MLC. We failed to see a significant increase in ROCK1/2, MYPT, or MLC expression (Fig 1D), suggesting that an increase in phospho-MYPT and phospho-MLC content was the result of the ROCK activation and downstream proteins phosphorylation rather than a result of protein levels alterations.

MLCK depletion attenuates LPS-induced MLC phosphorylation and barrier dysfunction

We observed a transient increase of intracellular calcium in LPS-treated cells (Fig. 2A). We first questioned if this increase contributed to LPS-induced barrier compromise. For that, we pretreated HLMVEC with a cell-permeable calcium chelator BAPTA-AM. 2.5μM BAPTA-AM pretreatment attenuated the initial drop in TER (first 6 hours of response to LPS); however, TER values during the late phase of response to LPS (8–18h post-LPS addition) were lower in the presence of BAPTA-AM. These data suggest that changes in intracellular calcium are physiologically linked to both the deregulation of barrier by LPS and the consecutive barrier restoration (Fig. 2B).

To prove that MLCK, being one of the calcium-calmodulin effectors, is actively involved in the physiological response to LPS, we checked if the inhibition of MLCK by calcium chelator BAPTA-AM and selective inhibitor ML7 would have an effect on LPS-induced MLC phosphorylation. We observed that the pretreatment of HLMVEC with BAPTA-AM and ML7 attenuated LPS-induced increase in MLC mono-phosphorylation and decreased both basal and LPS-induced diphospho-MLC content (Fig. 2C and Fig 2 suppl). The effect of BAPTA-AM on MLC phosphorylation was more pronounced than the effect of ML7 at any time point. We next assessed how LPS-induced TER drop is affected by ML7 pretreatment. Preincubation with ML7 caused an abrupt loss of barrier function lasting for more than 30 min (data not shown). LPS added after barrier restoration caused TER drops of similar magnitude both in the presence or absence of ML7 (Fig. 2D).

We next checked if MLCK down-regulation by MLCK siRNA would have an effect on LPS-induced MLC phosphorylation and barrier compromise. *MYLK* gene is known to encode three major products: long non-muscle MLCK, short smooth-muscle MLCK, and a 17kDa protein telokin (Herring et al., 2006). In this study, we employed MYLK/MLCK siRNA, composed of a mixture of three strands, none of which was targeting telokin mRNA. As both non-muscle and smooth muscle MLCK are known to exist in endothelial cells (Garcia et al., 1997; Verin et al., 1998b), we first clarified what is the major MLCK isoform expressed in cultured HLMVEC. Using the three groups of primers, the first specific to the N-terminal extension of the non-muscle form of MLCK, the second specific for the region shared by both the non-muscle and smooth muscle MLCK, and the third specific to telokin, we were able to show that only short, smooth muscle isoform of MLCK is present in confluent HLMVEC or HUVEC (Fig 3A). We detected long non-muscle isoform only in over-confluent EC, suggesting that the expression of this isoform strongly depends on the maturity of endothelial monolayers. However, all the work done in this study was performed on confluent EC, limiting the analysis of MLCK involvement to the smooth muscle MLCK isoform.

Using real-time PCR with F2/R2 primers (detecting both isoforms of MLCK), we observed a strong down-regulation of MLCK mRNA level (down to less then 20%) in cells pretreated with 50nM MLCK siRNA (Fig. 3B). Using F2/R2, we also analyzed how LPS affected

MLCK mRNA level. Real-time PCR revealed that LPS increased MLCK mRNA level (Fig. 3C). The response was most apparent 24h post-LPS addition (~40% increase), but was also significant at earlier time points (6h, ~30% increase). RT-PCR with F1/R1 and F3/R3 primers (specific for the long MLCK isoform) failed to detect the appearance of the long isoform in LPS-treated cells, suggesting that the increase in MLCK mRNA seen by real-time PCR could be attributed to the changes in smooth-muscle MLCK mRNA level only.

To assess MLCK involvement in the regulation of barrier, we analyzed the effect of MLCK depletion on TER. We observed a moderate weakening of the basal barrier in cells pretreated with MLCK siRNA (Fig. 4A). When the cells were challenged with LPS, MLCK depletion attenuated LPS-induced drop in TER compared to the drop exhibited by control monolayers (Fig. 4B). We next analyzed MLC phosphorylation level and found that the effect of MLCK depletion can be seen on basal and LPS-induced levels of phospho-MLC (Fig 4 C, D). To reveal the effect of MLCK depletion on LPS-induced increase in MLC phosphorylation, we expressed the data as fold increase over the corresponding un-challenged control in each siRNA group (Fig 4 suppl). We found that MLCK depletion suppressed LPS-induced increase in both mono-and diphospho-MLC. Taken together with the effect of MLCK siRNA on LPS-induced drop in TER, these data suggest that MLCK-mediated increase in MLC phosphorylation contributes to the development of LPS-induced barrier dysfunction.

ROCK isoform depletion attenuates LPS-induced MLC phosphorylation and barrier dysfunction

To ascertain the contribution of individual ROCK isoforms in HLMVEC barrier regulation, we employed siRNAs specific to ROCK1 and ROCK2. We observed that ROCK1/2 siRNA pretreatments specifically suppressed the corresponding ROCK isoform expression without an effect on an alternative ROCK isoform expression (Fig. 5 suppl). The analysis of the basal TER in the cell pretreated with the specific ROCK siRNAs revealed that ROCK1 depletion significantly strengthened the endothelial barrier in the quiescent cells, whereas ROCK2 depletion did not have a noticeable effect on the basal TER value. Pretreatment with the combination of ROCK1 and 2 siRNA markedly decreased basal TER value 48h post-tranfection (Fig 5A), resulting in even more significant compromise within the next 24h (TER value 0.64±0.047 of basal TER of NS-pretreated cells).

The analysis of the monolayers response to LPS revealed that ROCK2, but not ROCK1 depletion significantly alleviated LPS-induced barrier compromise (Fig. 5B). The analysis of the double knockdown effect was hindered by the fact that ROCK1+2-depleted cells were not able to maintain the basal resistance level required to perform the assay.

The examination of the MLC phosphorylation level showed that ROCK2 depletion significantly suppressed LPS-induced increase in MLC mono-phosphorylation (Fig 5C, Fig 5 suppl). On contrary, ROCK1 depletion suppressed phospho-MLC level both in un-stimulated and stimulated cells, failing to suppress LPS-induced increase in MLC phosphorylation per se (Fig 5C, D, Fig 5 suppl). Altogether, these data suggest that whereas both ROCK 1 and 2 take part in the regulation of MLC level in HLMVEC, only ROCK2 activity contributes to the LPS-induced drop in TER and LPS-induced changes in MLC phosphorylation.

ROCK inhibitors Y-27632 and GSK429286 exacerbate LPS-induced HLMVEC barrier dysfunction

To analyze whether pharmacological inhibition of ROCK would alleviate LPS-induced hyperpermeability, we employed a well-known ROCK inhibitor Y-27632 and a novel

ROCK-specific inhibitor GSK429286. The use of ROCK1/2 inhibitor Y-27632 in the experiments with slow-acting edemagenic factors was actively criticized due to the hindering effect of Y-27632 on basal permeability (van Nieuw Amerongen et al., 2007) and its relatively low specificity (Nichols et al., 2009). Aside from ROCK inhibition, Y-27632 is known to have a marked effect on the kinase PKN/PRK2. Novel inhibitor GSK429286 is more specific toward ROCK and does not inhibit PKN/PRK2 as effectively (Nichols et al., 2009). Pretreatment of HLMVEC monolayers with ROCK inhibitor Y-27632 (5μM) noticeably reduced baseline resistance across EC monolayer (Fig 6A). Contrary to our results with individual ROCK depletions, simultaneous inhibition of both ROCK1 and 2 with Y-27632 exacerbated LPS-induced changes in HLMVEC TER. Similar effects were observed in the experiments with FITC-dextran; namely, measurements of macromolecular tracer flux had shown that Y-27632 markedly increased permeability both in the presence and absence of LPS (Fig.6A, inset). Analogous to Y-27632, pretreatment with 0.5μM GSK429286 had significant compromising effect on the basal HLMVEC permeability. Accordingly, LPS-induced response was exacerbated in the presence of GSK429286 (Fig. 6B). To confirm that the concentration of GSK429286 used in our study effectively blocked ROCK-mediated responses, we studied the effect of GSK429286 pretreatment on the barrier compromise caused by the known ROCK inducer nocodazole. Of note, nocodazole-induced drop in TER was almost completely blocked in the presence of 0.5μM GSK429286 (Fig 6B, inset). These results clearly suggest that simultaneous inhibition of ROCK1 and 2 by the pharmacological inhibitors Y-27632 and GSK429286 is not beneficial for LPS-induced barrier hyperpermeability in HLMVEC monolayers.

To ascertain that the effect of Rho kinase inhibitors on TER was specific to the inhibition of MLC phosphorylation, we transfected cells with phosphorylation-deficient mutant of MLC. The wild-type and mutant xMLC-encoding constructs were conditionally expressed in HLMVEC infected with tTA-encoding adenovirus in the absence of doxycycline; the addition of doxycycline silenced the expression of MLC (Fig 6D). We observed that, comparable to monolayers pre-treated with Y-27632 and GSK429286, the monolayers overexpressing T18AS19A mutant exhibited lower basal resistance than control doxycycline-treated monolayers (Fig 6E). Significant drop in basal resistance (more than 20%) hindered the analysis of the response of these monolayers to LPS.

PKA activators attenuate LPS-induced HLMVEC responses

The decrease in cAMP was shown previously to be a part of the response to LPS in dermal microvascular endothelial cells (Schlegel et al., 2009). To show that inactivation of cAMP-dependent enzyme PKA, in fact, takes place in LPS-induced HLMVEC, we employed an antibody raised against PKA-specific phosphorylation sites. To validate the use of this antibody, we first analyzed the lysates from the quiescent cells and cells pretreated with PKA inhibitor H-89. As H-89 is also known to inhibit ROCK (Feng et al., 1999; Murray, 2008), we used Y-27632 pretreatment as an additional control. In lysates from quiescent cells, several bands were visible with the molecular weight ranging from 25 kDa to 200 kDa. We found that the intensity of the 95kDa band was significantly reduced by H-89, but not by Y-27632 pretreatment (Fig 7A). These results suggested that the antibody in use indeed detected the proteins phosphorylated by PKA.

Analysis of the lysates from LPS-stimulated HLMVEC revealed that the overall intensity of the staining was noticeably reduced in the cells treated with LPS for more than 2 hours (Fig. 7B). The reduction was especially obvious for the bands of ~130kDa, 95kDa, and 27 kDa. Pretreatment with adenylate cyclase activator, forskolin, and specific PKA activator, bnz-cAMP, resulted in the appearance of a novel phospho-band of ~125kDa (Fig. 7C, side arrow). In contrast, o-me-cAMP, an activator of another cAMP effector, Epac, did not have such effect. In addition, the LPS-induced decline of the intensity of 95kDa phospho-band

was significantly attenuated by forskolin and bnz-cAMP, but not by o-me-cAMP pretreatment (Fig. 7C, arrows on the gel).

Earlier we showed that the agents increasing cAMP level (forskolin and IBMX) or the agents specifically activating PKA (bnz-cAMP) alleviated LPS-induced hyperpermeability in HLMVEC monolayers (Bogatcheva et al., 2009). As MLC phosphorylation was known to be suppressed by the cAMP increase and PKA activation, we next analyzed how the level of phospho-MLC was altered in LPS-treated cells in the presence of PKA activators. We observed that the level of monophospho- and diphospho-MLC was significantly reduced in forskolin- and bnz-cAMP pretreated cells (Fig. 8A, B, D), indicating that PKA activation effectively suppressed the LPS-induced MLC phosphorylation in HLMVEC. The analysis of MYPT phosphorylation revealed no changes in pMYPT level in response to forskolin- and bnz-cAMP (Fig 8C, D). The latter fact let us suggest that PKA-mediated reduction of MLC phosphorylation was not critically dependent on the inactivation of the Rho/ROCK/MYPT pathway.

Y-27632 and bnz-cAMP have different effects on the LPS-induced redistribution of phospho-MLC signal

To understand why Y-27632-induced suppression of MLC phosphorylation was detrimental for LPS-compromised barrier, whereas forskolin- and bnz-cAMP-induced suppression had beneficial effect (Bogatcheva et al., 2009), we assessed the distribution of F-actin and diphospho-MLC in HLMVEC pretreated with these agents. In quiescent cells, diphospho-MLC signal forms a peripheral pattern coinciding with the localization of the cortical actin (Fig 9, upper panel). In the cells pretreated with Y-27632, this peripheral staining seems interrupted, with the areas of the apparent signal deficit (indicated by arrows). In contrast, bnz-cAMP pretreatment strengthens peripheral ppMLC signal (indicated by arrows) and increases the intensity of the merged ppMLC/F-actin signal (Fig 9 suppl) indicating the association of the peripheral ppMLC signal with the cortical actin structures. The analysis of the distribution profile of ppMLC signal across the cell (Fig 10) revealed that the thickness of the peripheral ppMLC staining is significantly increased in bnz-cAMP-pretreated cells.

LPS challenge induced stress fiber formation in HLMVEC. ppMLC signal in LPS-treated cells co-localized with stress fibers; cortical structures contributed only minor amount of signal (Fig 9, Fig 9 suppl, Fig 10). Y-27632 pretreatment completely suppressed LPS-induced stress fiber induction, whereas bnz-cAMP pretreatment had only moderate effect on this process (Fig 9, Fig 9 suppl, Fig 10). Notably, the thickness of the peripheral structures was significantly reduced in both Y-27632 and bnz-cAMP-pretreated cells in LPS-dependent manner (Fig 10). However, in the presence of LPS the thickness of the cortical structures in bnz-cAMP-pretreated cells was still significantly higher that that of control cells, whereas the thickness of cortical structures in Y-27632-pretreated cells was lower than that of control cells. These observations revealed the major differences between the effects of ROCK inhibitors and PKA activators on MLC phosphorylation-dependent actomyosin rearrangement in LPS-treated cells.

Discussion

In the first part of this study, we analyzed how the increase in MLC phosphorylation, mediated by different regulatory enzymes, contributed to the LPS-induced endothelial barrier dysfunction. We found that in HLMVEC monolayers, LPS stimulation caused an increase in MYPT phosphorylation and an elevation of intracellular calcium (Fig. 1, 2), likely resulting in the deactivation of myosin phosphatase and activation of MLCK by calcium-calmodulin. These changes preceded or coincided with the increase in phospho-MLC level, which, in turn, was concomitant with the onset of barrier hyperpermeability.

To ascertain that calcium elevation was relevant to the subsequent loss of endothelial barrier in LPS-treated cells, we employed a cell-permeable calcium chelator BAPTA-AM. We have shown that BAPTA-AM pretreatment delayed the loss of barrier function in LPS-treated cells, suggesting the involvement of calcium-dependent barrier-disruptive pathways in the response to LPS (Fig 2A). Subsequent deterioration of the barrier function in BAPTA-AM-pretreated cells could be explained by the inactivation of calcium-dependent barrier protective enzymes, such as calmodulin-dependent phosphatase calcineurin (PP2B) (Csortos et al., 2007; Verin et al., 1998a); future study will be needed to ascertain this mechanism.

We next examined the role of calcium/calmodulin-dependent MLC kinase MLCK in LPS-induced barrier dysfunction. We observed that the concentration of ML7 used in our study (10 μM) partially suppressed MLC phosphorylation, however, failed to alleviate LPS-induced barrier dysfunction. As pharmacological inhibitors ML7 and ML9 were recently criticized for their effects not related to the suppression of MLCK-dependent MLC phosphorylation (Watanabe et al., 2007), we chose to assess MLCK involvement using MLCK-specific siRNA rather than to increase ML7 concentration to the point where it is no longer MLCK-specific.

Two MLCK isoforms were shown to be expressed in endothelial cells, the shorter smooth-muscle 130kDa MLCK, and the longer non-muscle 250kDa MLCK (Garcia et al., 1997; Verin et al., 1998b). The two isoforms share all the functional domains necessary for the substrate recognition and regulation by calcium-calmodulin, implying certain redundancy in their function (Herring et al., 2006). In this study, we show that the longer isoform is not expressed in confluent cultured HLMVEC or HUVEC (Fig. 3), but is detectable in over-confluent endothelial cells. The fact that there are conditions when cultured HLMVEC do not express long MLCK isoform gave us a unique opportunity to analyze the specific role of the short, smooth muscle MLCK in endothelial dysfunction.

In confluent HLMVEC, the level of MLCK mRNA was efficiently down-regulated after 48h pretreatment with MLCK-specific siRNA. MLCK depletion significantly attenuated both the LPS-induced increase in MLC phosphorylation and the drop in TER (Fig. 4), attesting to the involvement of the smooth muscle MLCK in the development of LPS-induced barrier compromise. It was shown earlier that the non-muscle MLCK down-regulation attenuates LPS-induced vascular hyperpermeability in vitro and in vivo (Mirzapoiazova et al.; Wainwright et al., 2003). Altogether, these data suggest that both isoforms can contribute to the regulation of barrier permeability, and the role of the smooth-muscle MLCK in endothelium should not be overlooked. The fact that LPS increases the level of MLCK mRNA (Fig 3D) suggests that the barrier disruption mechanism evoked by LPS can engage not only MLCK activation, but also the up-regulation of MLCK expression level.

In the next step, we analyzed the involvement of the ROCK-dependent pathways in the LPS-induced barrier dysfunction. The analysis of the resistance of the quiescent monolayers, deficient for the individual ROCK isoforms, revealed that ROCK1 knockdown significantly improved basal barrier function. These results were consistent with the recent report (Finigan et al., 2009), showing that the protection from capillary leakage is associated with an attenuation of ROCK1 expression. Unlike ROCK1, ROCK2 knockdown did not have a significant effect on the basal HLMVEC barrier, whereas simultaneous depletion of both isoforms resulted in the dramatic loss of barrier function (about 25% decrease 48h post-transfection with further decline); these results were similar to those obtained in HUVEC (van Nieuw Amerongen et al., 2007). The analysis of the response of monolayers deficient for individual ROCK isoforms revealed that ROCK2, but not ROCK1 knockdown, has a pronounced effect on LPS-induced MLC phosphorylation and barrier dysfunction (Fig. 5). Earlier, it was shown that ROCK2, but not ROCK1 mediated the disassembly of epithelial

junctions in response to calcium depletion (Samarin et al., 2007). Altogether, these data prove that both ROCK1 and ROCK2 take part in the regulation of pulmonary barrier; however, the contribution of these isoforms in the basal maintenance and induced dysfunction is different. Recently, Rho/ROCK activation in dermal microvascular endothelial cells was suggested to be of minor importance for the LPS-induced barrier compromise based on the fact that this activation occurred late in the course of response when barrier dysfunction had already developed (Schlegel et al., 2009). Our data provide evidence that in pulmonary microvascular EC, Rho/ROCK-dependent MLC phosphorylation is linked to the LPS-induced loss of barrier both temporally and functionally, coinciding with the onset in hyperpermeability and contributing to it.

We next analyzed if the pharmacological inhibition of ROCK would have a beneficial effect on the LPS-compromised barrier (Fig. 6). We observed that, contrary to the effects of individual ROCK depletions, the indiscriminate inhibition of both isoforms by the inhibitors Y-27632 and GSK429286 led to the deterioration of the basal and LPS-compromised barrier. These results were consistent with the fact that double ROCK knock-down results in a severe barrier leak (Fig. 5). Analysis of ROCK inhibitors' effects on MLC phosphorylation revealed that, unlike ROCK siRNAs, which mostly affected an increase in MLC monophosphorylation, Y-27632 also had a strong effect on MLC diphosphorylation. Of note, preferential inhibition of MLC-diphosphorylation versus monophosphorylation by Y-27632 was described before in epithelial cells (Watanabe et al., 2007). Analogous to Y-27632 and GSK429286 pre-treatments, the overexpression of the phosphorylation-deficient MLC mutant significantly lowered the resistance across HLMVEC monolayer (Fig 6D). These data confirmed that the effect of Y-27632 and GSK429286 on TER should be attributed to the inhibition of MLC phosphorylation rather than phosphorylation of some other ROCK substrates. Disparate effects of individual ROCK knock-downs versus ROCK1/2 simultaneous inhibition let us suggest that the involvement of Rho kinases in any cellular function should not be evaluated solely based on the effects of ROCK inhibitors. In regard to barrier permeability, our results clearly suggest that despite the involvement of ROCK into the regulation of MLC phosphorylation and barrier function, neither Y-27632 nor GSK429286 could be used as pharmacological tools to alleviate LPS-induced hyperpermeability in human endothelium.

The next question we asked is whether PKA-dependent pathways are involved in the modulation of phospho-MLC-dependent contractile activity in response to LPS. A decrease in cAMP level was shown in dermal microvascular endothelial cells challenged with LPS (Schlegel et al., 2009). However, earlier described differences in temporal activation of Rho/ROCK pathways let us suggest that pulmonary and dermal endothelial cells could vary in more than one signaling mechanism. We first showed that LPS caused a time-dependent decrease in the phosphorylation level of protein-substrates for PKA (Fig. 7). For certain protein bands, this decrease could be counteracted by the elevation of cAMP level or by specific activation of PKA by the cAMP analogue bnz-cAMP. In addition, forskolin or bnz-cAMP pretreatment induced the phosphorylation of the bands which were not phosphorylated in quiescent cells. These data prove that PKA-dependent pathways are down-regulated in HLMVEC responding to LPS, and pharmacological elevation of cAMP level or specific activation of PKA can over-ride certain effects of LPS.

There is no shortage of data about possible mechanisms by which PKA can down-regulate MLC phosphorylation and contraction. These involve phosphorylation and inactivation of MLCK (Nishikawa et al., 1984), inactivation of Rho (Murray, 2008), and an effect on phosphatase1 catalytic subunit distribution to the myosin fraction (Bindewald et al., 2004). Here we showed that both mono- and di-phosphorylation of MLC were affected by cAMP elevation or specific activation of PKA. Together with the earlier published results

demonstrating that forskolin and bnz-cAMP pretreatment blocks the LPS-induced drop in TER (Bogatcheva et al., 2009), our data suggest that the suppression of MLC phosphorylation could be one of the plausible mechanisms by which PKA alleviates barrier compromise in endothelium exposed to LPS. The absence of the pronounced effect of forskolin/bnz-cAMP on LPS-induced MYPT phosphorylation indicated that cAMP-dependent inhibition of the Rho/ROCK/MYPT pathway is not a major event mediating the effect of forskolin/bnz-cAMP on MLC phosphorylation (Fig 8).

In an attempt to understand why Y-27632-mediated decrease in MLC phosphorylation is detrimental to the barrier, while forskolin and bnz-cAMP-mediated decrease is beneficial, we assessed the di-phospho-MLC distribution in the quiescent and LPS-challenged monolayers. In the absence of inhibitors/activators, LPS caused overall increase in F-actin/ppMLC signal concomitant with the disappearance of prominent cortical structures and an induction of stress fiber formation (Fig 9, 9 suppl, 10). We observed that Y-27632, while completely suppressing stress fiber formation in LPS-treated cells, preserved certain amount of ppMLC signal originating from cortical structures. However, this amount was significantly lower comparing to the amount detected in un-challenged cells. On the contrary, bnz-cAMP, having only moderate effect on the stress fiber formation, strengthened cortical association of ppMLC signal both in the absence and presence of LPS. It is possible therefore that under challenges such as LPS, the preservation of the strong association between ppMLC and the cortical actomyosin structures is more critical for the barrier maintenance than the suppression of relatively moderate stress fiber formation. Our results clearly indicate that the decrease in overall MLC phosphorylation, induced by the certain pharmacological agents, is not necessarily barrier protective. Hence, the western blot analysis with phospho-MLC antibody could be very misleading and should not be interpreted without the analysis of intracellular phospho-MLC distribution.

It is interesting to discuss the effect of MLC di-phosphorylation on the state of actomyosin cytoskeleton. It was long believed that mono-phosphorylation is the driving force behind stress fiber formation and contraction in smooth muscle and non-muscle cells, while di-phosphorylation plays subsidiary role to gain the maximum contraction (Ikebe and Hartshorne, 1985; Ikebe et al., 1988; Itoh et al., 1992). However, recent study on the three-dimensional distribution of phosphorylated MLC had shown that diphospho-MLC could differ from monophospho-MLC in localization, implying that functional differences may be deeper than just potentiation of contraction. In motile HeLa cells, diphospho-MLC are localized at the base of the leading edge, spatially very close to the substrate, whereas mono-phospho-MLC inhabit the tip of the filopodia and the top of the cell leading edge (Uchimura et al., 2002). The study utilizing MLC mutants, mimicking mono- and diphosphorylation, showed that diphosphorylation slowed down the degree of myosin turnover more markedly than monophosphorylation, contributing to the stabilization of actomyosin structures (Watanabe et al., 2007). One could speculate that ppMLC distribution in the peripheral actomyosin structures could serve to stabilize these structures and their attachment to the substrate, necessary for the maintenance of the endothelial barrier. These data suggest that a comparative assessment of MLC di- and mono-phosphorylation could render useful information about the nature of actomyosin rearrangement at certain locales.

Undoubtedly, the redistribution of the diphospho-MLC signal in HLMVEC would not be the sole barrier-protective mechanism exerted by PKA activation. Recently we have shown that PKA-dependent VASP phosphorylation contributes to the alleviation of LPS-induced barrier compromise (Bogatcheva et al., 2009). We speculate that PKA-dependent strengthening of the cortical actomyosin structures along with the reinforcement of their VASP-mediated anchoring via ZO-1 and VE-cadherin are the coordinated events of one barrier-protective mechanism opposing cell contraction and gap formation in endothelial monolayer.

In summary, here we demonstrate that the smooth muscle MLCK- and ROCK2-dependent changes in MLC phosphorylation contribute to the LPS-induced barrier dysfunction; however, current pharmacological inhibitors of these enzymes are ineffective or detrimental to the human pulmonary endothelium barrier function. cAMP elevator forskolin and PKA activator bnz-cAMP, known to alleviate LPS-induced barrier compromise, suppress LPS-induced MLC phosphorylation. However, unlike Y-27632-mediated suppression of the overall LPS-induced phosphorylation, PKA activation results in the strengthening of the peripheral diphospho-MLC signal. The latter event is more likely to evoke barrier protection in LPS-challenged monolayers than the suppression of the stress fiber formation per se. These data contribute to our understanding of the complex rearrangements of the actomyosin state induced by MLCK and ROCK inhibition and PKA activation, and their functional significance.

Supplementary Material

Refer to Web version on PubMed Central for supplementary material.

Acknowledgments

The authors are grateful to Dr. E. Zemskov for the valuable discussion of the manuscript, and to Ms. J. Gallops and Mr. Y. Kovalenkov for the technical assistance with preparation of manuscript and some of the experiments. We thank Mrs. C. Snead and Dr. J. Catravas for the culture of HUVEC cells, and Dr. Bujard for pUHD10-3 vector. Aside from the grants listed before, this work was also supported by a Programmatic Development Award from Cardiovascular Discovery Institute of Medical College of Georgia.

Contract grant sponsor: National Heart, Lung and Blood Institute

Contract grant numbers: HL-080675, HL-083327, HL-067307

Contract grant sponsor: American Heart Association

Contract grant number: SDG 0930038N

Literature cited

Bindewald K, Gunduz D, Hartel F, Peters SC, Rodewald C, Nau S, Schafer M, Neumann J, Piper HM, Noll T. Opposite effect of cAMP signaling in endothelial barriers of different origin. Am J Physiol Cell Physiol. 2004; 287(5):C1246–C1255. [PubMed: 15475517]

Bogatcheva NV, Verin AD. The role of cytoskeleton in the regulation of vascular endothelial barrier function. Microvasc Res. 2008; 76(3):202–207. [PubMed: 18657550]

Bogatcheva NV, Zemskova MA, Kovalenkov Y, Poirier C, Verin AD. Molecular mechanisms mediating protective effect of cAMP on lipopolysaccharide (LPS)-induced human lung microvascular endothelial cells (HLMVEC) hyperpermeability. J Cell Physiol. 2009; 221(3):750–759. [PubMed: 19725051]

Bresnick AR, Wolff-Long VL, Baumann O, Pollard TD. Phosphorylation on threonine-18 of the regulatory light chain dissociates the ATPase and motor properties of smooth muscle myosin II. Biochemistry. 1995; 34(39):12576–12583. [PubMed: 7548006]

Comerford KM, Lawrence DW, Synnestvedt K, Levi BP, Colgan SP. Role of vasodilator-stimulated phosphoprotein in PKA-induced changes in endothelial junctional permeability. Faseb J. 2002; 16(6):583–585. [PubMed: 11919161]

Csortos C, Kolosova I, Verin AD. Regulation of vascular endothelial cell barrier function and cytoskeleton structure by protein phosphatases of the PPP family. Am J Physiol Lung Cell Mol Physiol. 2007; 293(4):L843–L854. [PubMed: 17693486]

da Silva-Santos JE, Chiao CW, Leite R, Webb RC. The Rho-A/Rho-kinase pathway is up-regulated but remains inhibited by cyclic guanosine monophosphate-dependent mechanisms during

endotoxemia in small mesenteric arteries. Crit Care Med. 2009; 37(5):1716–1723. [PubMed: 19325475]

Essler M, Staddon JM, Weber PC, Aepfelbacher M. Cyclic AMP blocks bacterial lipopolysaccharide-induced myosin light chain phosphorylation in endothelial cells through inhibition of Rho/Rho kinase signaling. J Immunol. 2000; 164(12):6543–6549. [PubMed: 10843713]

Eutamene H, Theodorou V, Schmidlin F, Tondereau V, Garcia-Villar R, Salvador-Cartier C, Chovet M, Bertrand C, Bueno L. LPS-induced lung inflammation is linked to increased epithelial permeability: role of MLCK. Eur Respir J. 2005; 25(5):789–796. [PubMed: 15863634]

Feng J, Ito M, Kureishi Y, Ichikawa K, Amano M, Isaka N, Okawa K, Iwamatsu A, Kaibuchi K, Hartshorne DJ, Nakano T. Rho-associated kinase of chicken gizzard smooth muscle. J Biol Chem. 1999; 274(6):3744–3752. [PubMed: 9920927]

Finigan JH, Boueiz A, Wilkinson E, Damico R, Skirball J, Pae HH, Damarla M, Hasan E, Pearse DB, Reddy SP, Grigoryev DN, Cheadle C, Esmon CT, Garcia JG, Hassoun PM. Activated protein C protects against ventilator-induced pulmonary capillary leak. Am J Physiol Lung Cell Mol Physiol. 2009; 296(6):L1002–L1011. [PubMed: 19363121]

Fukata Y, Amano M, Kaibuchi K. Rho-Rho-kinase pathway in smooth muscle contraction and cytoskeletal reorganization of non-muscle cells. Trends Pharmacol Sci. 2001; 22(1):32–39. [PubMed: 11165670]

Garcia JG, Lazar V, Gilbert-McClain LI, Gallagher PJ, Verin AD. Myosin light chain kinase in endothelium: molecular cloning and regulation. Am J Respir Cell Mol Biol. 1997; 16(5):489–494. [PubMed: 9160829]

Goeckeler ZM, Wysolmerski RB. Myosin light chain kinase-regulated endothelial cell contraction: the relationship between isometric tension, actin polymerization, and myosin phosphorylation. J Cell Biol. 1995; 130(3):613–627. [PubMed: 7622562]

Herring BP, El-Mounayri O, Gallagher PJ, Yin F, Zhou J. Regulation of myosin light chain kinase and telokin expression in smooth muscle tissues. Am J Physiol Cell Physiol. 2006; 291(5):C817–C827. [PubMed: 16774989]

Ikebe M, Hartshorne DJ. Phosphorylation of smooth muscle myosin at two distinct sites by myosin light chain kinase. J Biol Chem. 1985; 260(18):10027–10031. [PubMed: 3839510]

Ikebe M, Koretz J, Hartshorne DJ. Effects of phosphorylation of light chain residues threonine 18 and serine 19 on the properties and conformation of smooth muscle myosin. J Biol Chem. 1988; 263(13):6432–6437. [PubMed: 2966156]

Itoh K, Hara T, Shibata N. Diphosphorylation of platelet myosin by myosin light chain kinase. Biochim Biophys Acta. 1992; 1133(3):286–292. [PubMed: 1531301]

Jacobson JR, Garcia JG. Novel therapies for microvascular permeability in sepsis. Curr Drug Targets. 2007; 8(4):509–514. [PubMed: 17430121]

Kamm KE, Stull JT. Dedicated myosin light chain kinases with diverse cellular functions. J Biol Chem. 2001; 276(7):4527–4530. [PubMed: 11096123]

Kolosova IA, Mirzapoiazova T, Moreno-Vinasco L, Sammani S, Garcia JG, Verin AD. Protective effect of purinergic agonist ATPgammaS against acute lung injury. Am J Physiol Lung Cell Mol Physiol. 2008; 294(2):L319–L324. [PubMed: 17993588]

Komarova Y, Malik AB. Regulation of endothelial permeability via paracellular and transcellular transport pathways. Annu Rev Physiol. 2010; 72:463–493. [PubMed: 20148685]

Kooistra MR, Corada M, Dejana E, Bos JL. Epac1 regulates integrity of endothelial cell junctions through VE-cadherin. FEBS Lett. 2005; 579(22):4966–4972. [PubMed: 16115630]

Lorenowicz MJ, Fernandez-Borja M, Hordijk PL. cAMP signaling in leukocyte transendothelial migration. Arterioscler Thromb Vasc Biol. 2007; 27(5):1014–1022. [PubMed: 17347487]

Lundblad C, Bentzer P, Grande PO. The permeability-reducing effects of prostacyclin and inhibition of Rho kinase do not counteract endotoxin-induced increase in permeability in cat skeletal muscle. Microvasc Res. 2004; 68(3):286–294. [PubMed: 15501248]

Martin, GS.; Bernard, GR. Management of respiratory dysfunction in patients with severe sepsis. In: Vincent, J-L.; Carlet, J.; Opal, SM., editors. The sepsis text. Boston Dordrecht London: Kluwer Academic Publishers; 2002. p. 455-477.

Martin GS, Mannino DM, Eaton S, Moss M. The epidemiology of sepsis in the United States from 1979 through 2000. N Engl J Med. 2003; 348(16):1546–1554. [PubMed: 12700374]

Matsumura F, Hartshorne DJ. Myosin phosphatase target subunit: Many roles in cell function. Biochem Biophys Res Commun. 2008; 369(1):149–156. [PubMed: 18155661]

Mirzapoiazova T, Moitra J, Moreno-Vinasco L, Sammani S, Turner JR, Chiang ET, Evenoski C, Wang T, Singleton PA, Huang Y, Lussier YA, Watterson DM, Dudek SM, Garcia JG. The Non Muscle Myosin Light Chain Kinase Isoform is a Viable Molecular Target in Acute Inflammatory Lung Injury. Am J Respir Cell Mol Biol. 2010

Mong PY, Wang Q. Activation of Rho kinase isoforms in lung endothelial cells during inflammation. J Immunol. 2009; 182(4):2385–2394. [PubMed: 19201893]

Moriez R, Salvador-Cartier C, Theodorou V, Fioramonti J, Eutamene H, Bueno L. Myosin light chain kinase is involved in lipopolysaccharide-induced disruption of colonic epithelial barrier and bacterial translocation in rats. Am J Pathol. 2005; 167(4):1071–1079. [PubMed: 16192642]

Murray AJ. Pharmacological PKA inhibition: all may not be what it seems. Sci Signal. 2008; 1(22):re4. [PubMed: 18523239]

Nichols RJ, Dzamko N, Hutti JE, Cantley LC, Deak M, Moran J, Bamborough P, Reith AD, Alessi DR. Substrate specificity and inhibitors of LRRK2, a protein kinase mutated in Parkinson's disease. Biochem J. 2009; 424(1):47–60. [PubMed: 19740074]

Nishikawa M, de Lanerolle P, Lincoln TM, Adelstein RS. Phosphorylation of mammalian myosin light chain kinases by the catalytic subunit of cyclic AMP-dependent protein kinase and by cyclic GMP-dependent protein kinase. J Biol Chem. 1984; 259(13):8429–8436. [PubMed: 6547441]

Opal SM. The host response to endotoxin, antilipopolysaccharide strategies, and the management of severe sepsis. Int J Med Microbiol. 2007; 297(5):365–377. [PubMed: 17452016]

Qiao J, Huang F, Lum H. PKA inhibits RhoA activation: a protection mechanism against endothelial barrier dysfunction. Am J Physiol Lung Cell Mol Physiol. 2003; 284(6):L972–L980. [PubMed: 12588708]

Samarin SN, Ivanov AI, Flatau G, Parkos CA, Nusrat A. Rho/Rho-associated kinase-II signaling mediates disassembly of epithelial apical junctions. Mol Biol Cell. 2007; 18(9):3429–3439. [PubMed: 17596509]

Schlegel N, Baumer Y, Drenckhahn D, Waschke J. Lipopolysaccharide-induced endothelial barrier breakdown is cyclic adenosine monophosphate dependent in vivo and in vitro. Crit Care Med. 2009; 37(5):1735–1743. [PubMed: 19325485]

Tasaka S, Koh H, Yamada W, Shimizu M, Ogawa Y, Hasegawa N, Yamaguchi K, Ishii Y, Richer SE, Doerschuk CM, Ishizaka A. Attenuation of endotoxin-induced acute lung injury by the Rho-associated kinase inhibitor, Y-27632. Am J Respir Cell Mol Biol. 2005; 32(6):504–510. [PubMed: 15778497]

Uchimura T, Fumoto K, Yamamoto Y, Ueda K, Hosoya H. Spatial localization of mono-and diphosphorylated myosin II regulatory light chain at the leading edge of motile HeLa cells. Cell Struct Funct. 2002; 27(6):479–486. [PubMed: 12576640]

van Nieuw Amerongen GP, Beckers CM, Achekar ID, Zeeman S, Musters RJ, van Hinsbergh VW. Involvement of Rho kinase in endothelial barrier maintenance. Arterioscler Thromb Vasc Biol. 2007; 27(11):2332–2339. [PubMed: 17761936]

Verin AD, Birukova A, Wang P, Liu F, Becker P, Birukov K, Garcia JG. Microtubule disassembly increases endothelial cell barrier dysfunction: role of MLC phosphorylation. Am J Physiol Lung Cell Mol Physiol. 2001; 281(3):L565–L574. [PubMed: 11504682]

Verin AD, Cooke C, Herenyiova M, Patterson CE, Garcia JG. Role of Ca2+/calmodulin-dependent phosphatase 2B in thrombin-induced endothelial cell contractile responses. Am J Physiol. 1998a; 275(4 Pt 1):L788–L799. [PubMed: 9755112]

Verin AD, Lazar V, Torry RJ, Labarrere CA, Patterson CE, Garcia JG. Expression of a novel high molecular-weight myosin light chain kinase in endothelium. Am J Respir Cell Mol Biol. 1998b; 19(5):758–766. [PubMed: 9806740]

Wainwright MS, Rossi J, Schavocky J, Crawford S, Steinhorn D, Velentza AV, Zasadzki M, Shirinsky V, Jia Y, Haiech J, Van Eldik LJ, Watterson DM. Protein kinase involved in lung injury

susceptibility: evidence from enzyme isoform genetic knockout and in vivo inhibitor treatment. Proc Natl Acad Sci U S A. 2003; 100(10):6233–6238. [PubMed: 12730364]

Ware LB, Matthay MA. The acute respiratory distress syndrome. N Engl J Med. 2000; 342(18):1334–1349. [PubMed: 10793167]

Watanabe T, Hosoya H, Yonemura S. Regulation of myosin II dynamics by phosphorylation and dephosphorylation of its light chain in epithelial cells. Mol Biol Cell. 2007; 18(2):605–616. [PubMed: 17151359]

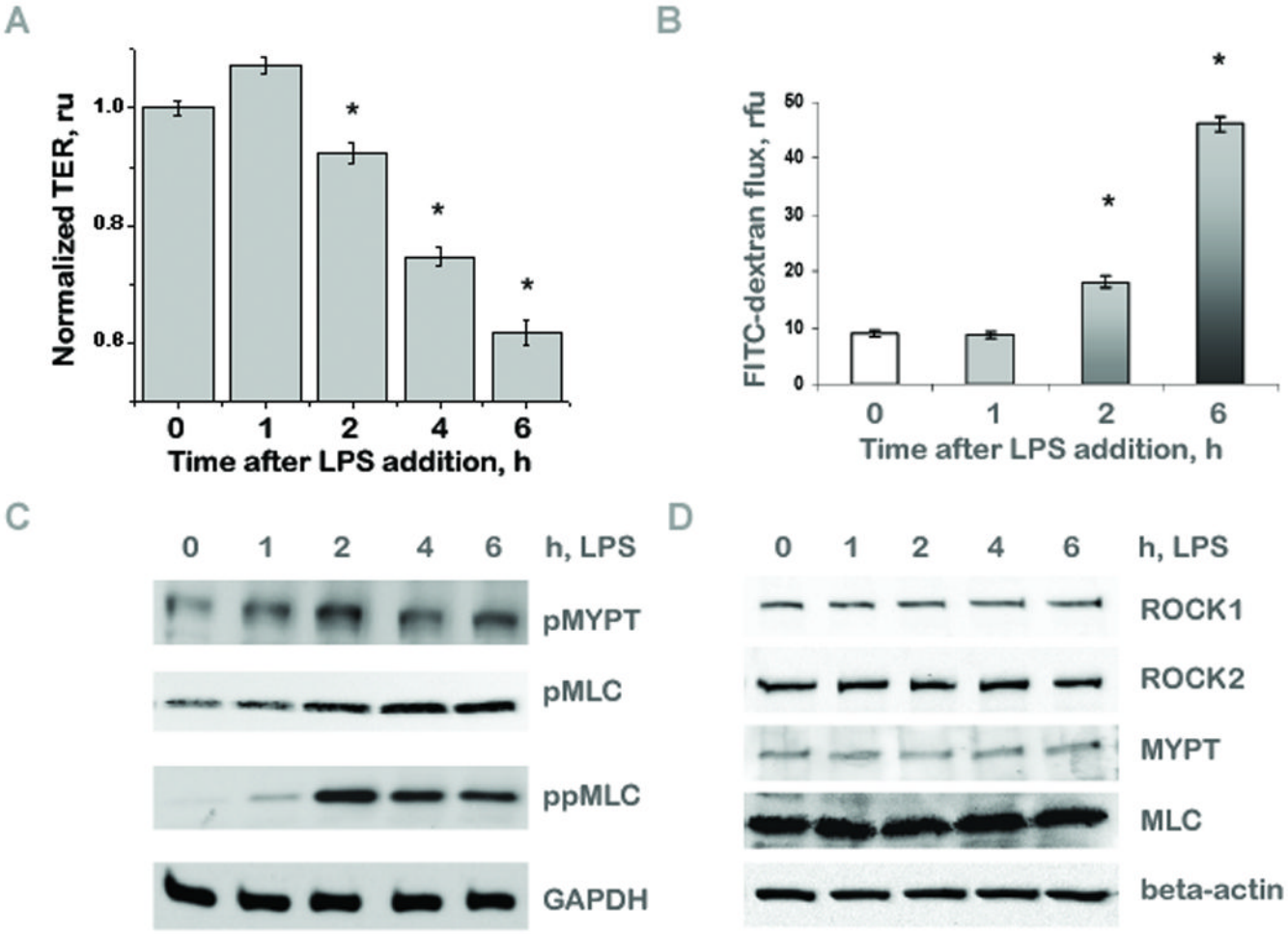

Fig. 1.

LPS evokes endothelial hyperpermeability and increases MLC phosphorylation. A, B: Human lung microvascular endothelial cells (HLMVEC) grown on the gold electrodes (A) or the semi-permeable collagenated nylon membrane inserts (B) were challenged with 100 ng/ml LPS for the time indicated. Transendothelial resistance (TER) values were normalized to the time point preceding LPS addition. Permeability of FITC-dextran across the cell monolayer was assessed as fluorescence of the media in the lower chambers. Shown are the means±SE of 3 parallel experiments. * indicates significant differences ($p<0.05$) with the samples before LPS addition (A) or samples, not challenged with LPS (B). C, D: HLMVEC grown in the wells of the 6-well plates were challenged with 100 ng/ml LPS for the time indicated, extracted and analyzed with (C) anti-pMLC, anti-ppMLC and anti-pMYPT antibodies, with GAPDH staining as a loading control or with (D) anti-ROCK1, anti-ROCK2, anti-MYPT and anti-MLC antibodies, with β-actin staining as a loading control. Shown are the representative Western blots out of 3 parallel experiments. Challenge with LPS results in the time-dependent loss of HLMVEC barrier integrity and increase in mono-phospho-MLC, di-phospho-MLC and phospho-MYPT content.

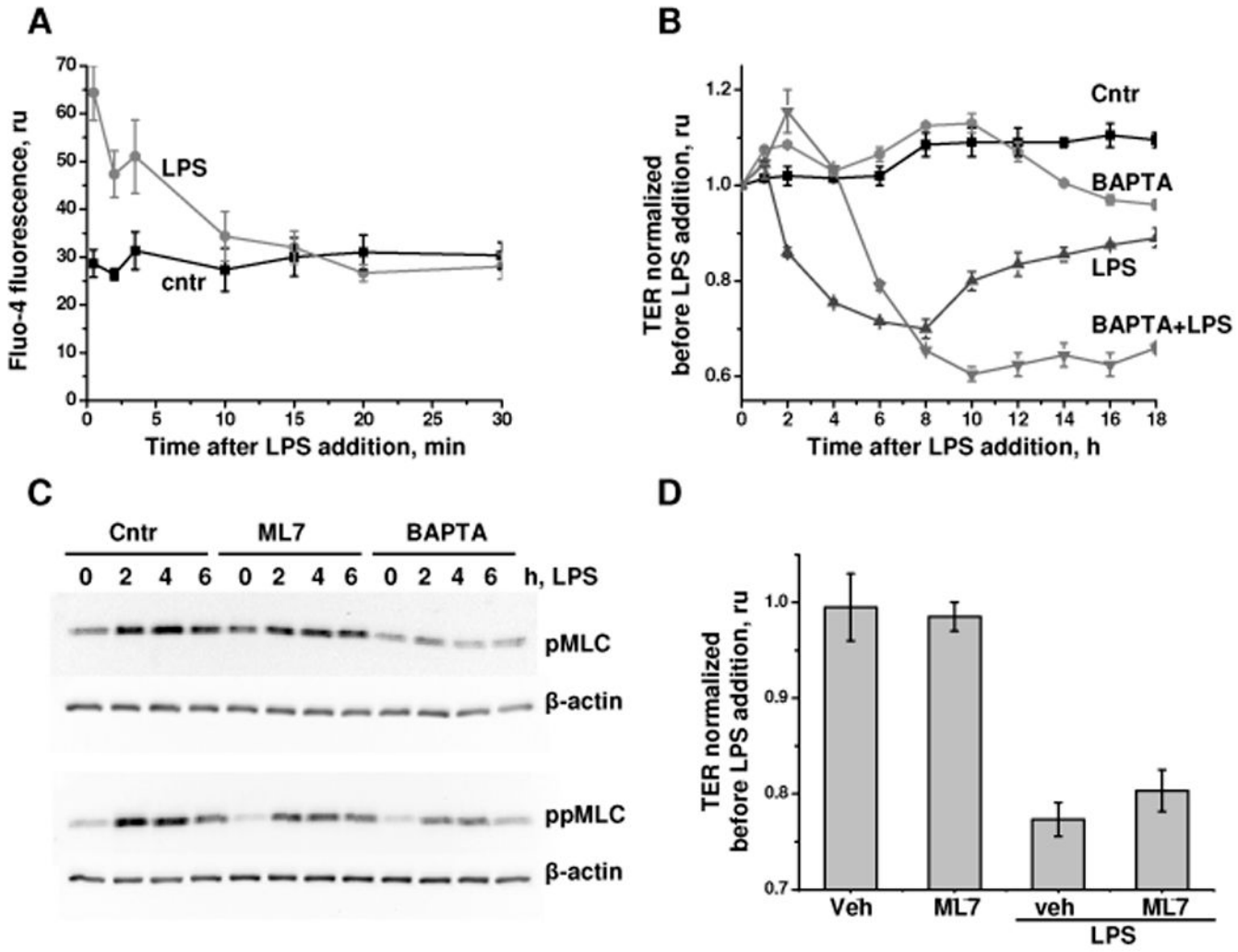

Fig. 2.

The effect of calcium chelator and MLCK inhibitor on LPS-induced TER decline and MLC phosphorylation. A: HLMVEC grown in the wells of 96-well plate were preloaded with Fluo-4 and challenged with 100ng/ml LPS (circles) or vehicle control (squares). B: HLMVEC grown on the gold electrodes were pretreated with vehicle control (squares, triangles) or 2.5μM BAPTA-AM (circles, inverse triangles) for 15 min, then challenged with 100 ng/ml LPS (triangles and inverse triangles). TER values were normalized to the time point preceding BAPTA-AM addition C: HLMVEC grown in the wells of the 12-well plates were pretreated with vehicle control, 10μM ML7, or 2.5μM BAPTA-AM for 15 min, then challenged with 100 ng/ml LPS for the time indicated, extracted and analyzed with anti-mono, anti-di-phospho-MLC and β-actin antibodies. Shown are representative Western Blots (n=3). For the normalized band intensities, please refer to Fig 2 suppl. D: HLMVEC were pretreated with vehicle control or 10μM ML7 for 15 min, then challenged with 100ng/ml LPS for 4h. TER values were normalized to the time point preceding ML7 addition. Similar results (no significant difference between vehicle- and ML7-pretreated groups) were obtained at 2h and 6h post-LPS addition. Shown are the (n=4 for A, n= 3 for B and D). * indicates significant differences ($p<0.05$) with the corresponding LPS time point pre-treated with vehicle control. LPS causes an increase of intracellular calcium in HLMVEC. Chelation of the intracellular calcium with BAPTA-AM affects both LPS-induced

hyperpermeability and MLC phosphorylation, while an inhibition of MLCK with ML7 affects MLC phosphorylation only.

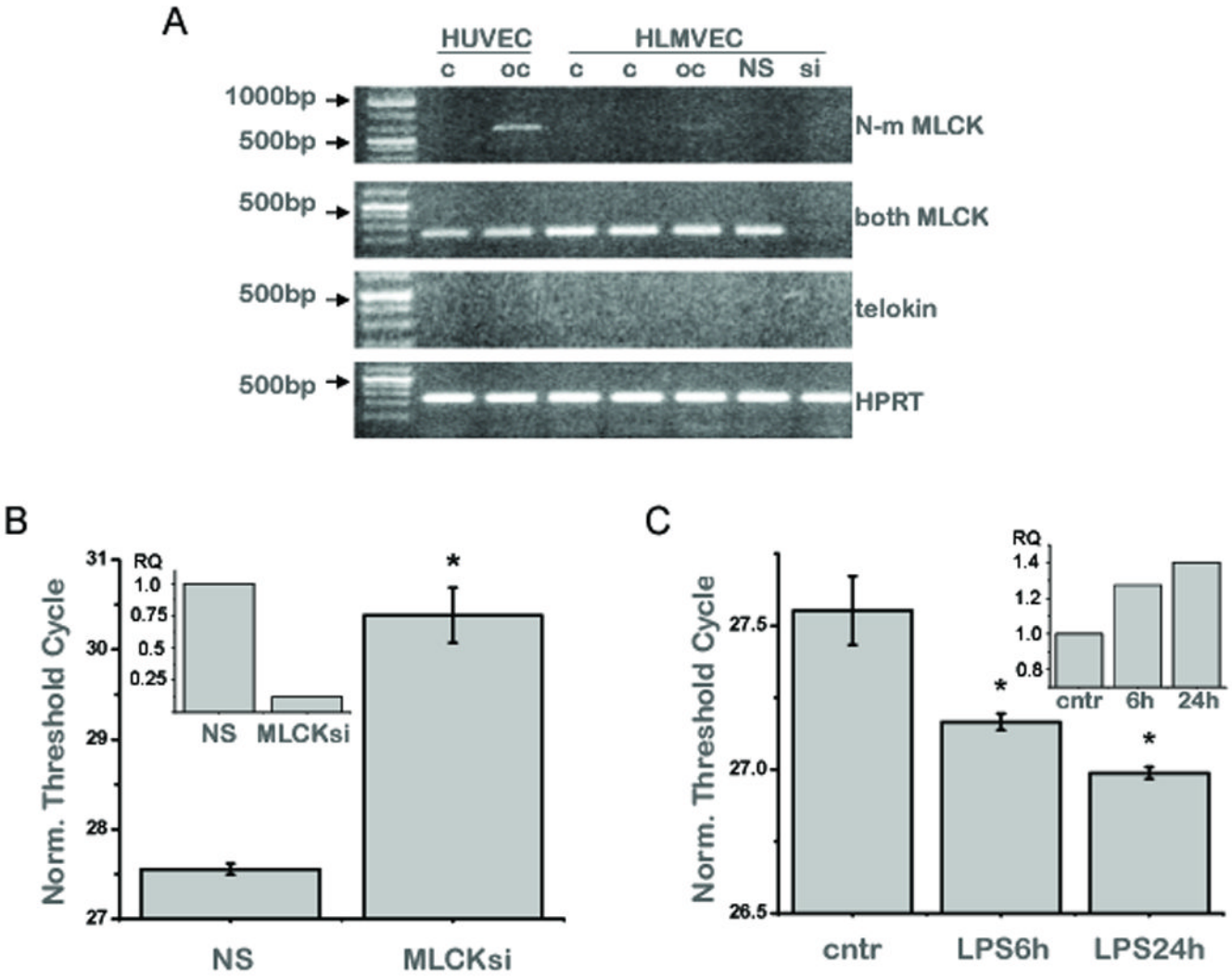

Fig. 3.

Down-regulation of MLCK mRNA and protein level in HLMVEC with the specific siRNA. A: HUVEC and HLMVEC confluent (c) and over-confluent (oc) monolayers, and HLMVEC pretreated with the non-silencing (NS) and MLCK siRNA (si) were subjected to RNA extraction. Monolayer confluence was assessed as described in Materials and Methods. MYLK F3/R3 primers were used to detect long, non-muscle MLCK mRNA. Similar results were obtained with other primers specific for the non-muscle MLCK. B: HLMVEC pretreated with 50nM MLCK siRNA (MLCKsi) or non-silencing RNA (NS) were lysed to extract RNA. B: mRNA level of MLCK was measured by real-time PCR using MYLK F2/R2 primers (non-discriminating between the non-muscle and smooth muscle MLCK) with HPRT as a control. Shown are the threshold cycle values (means±SE, n=3) and relative fold difference (inset) between the samples from NS and MLCKsi-pretreated cells. * indicates significant differences ($p<0.05$) with NS control. C: HLMVEC pretreated with 100ng/ml LPS for the time indicated were lysed to extract the RNA. Analysis was done as described in (B). MLCK siRNA pretreatment effectively knocks down smooth muscle MLCK mRNA in HLMVEC. LPS treatment causes an increase in MLCK mRNA level.

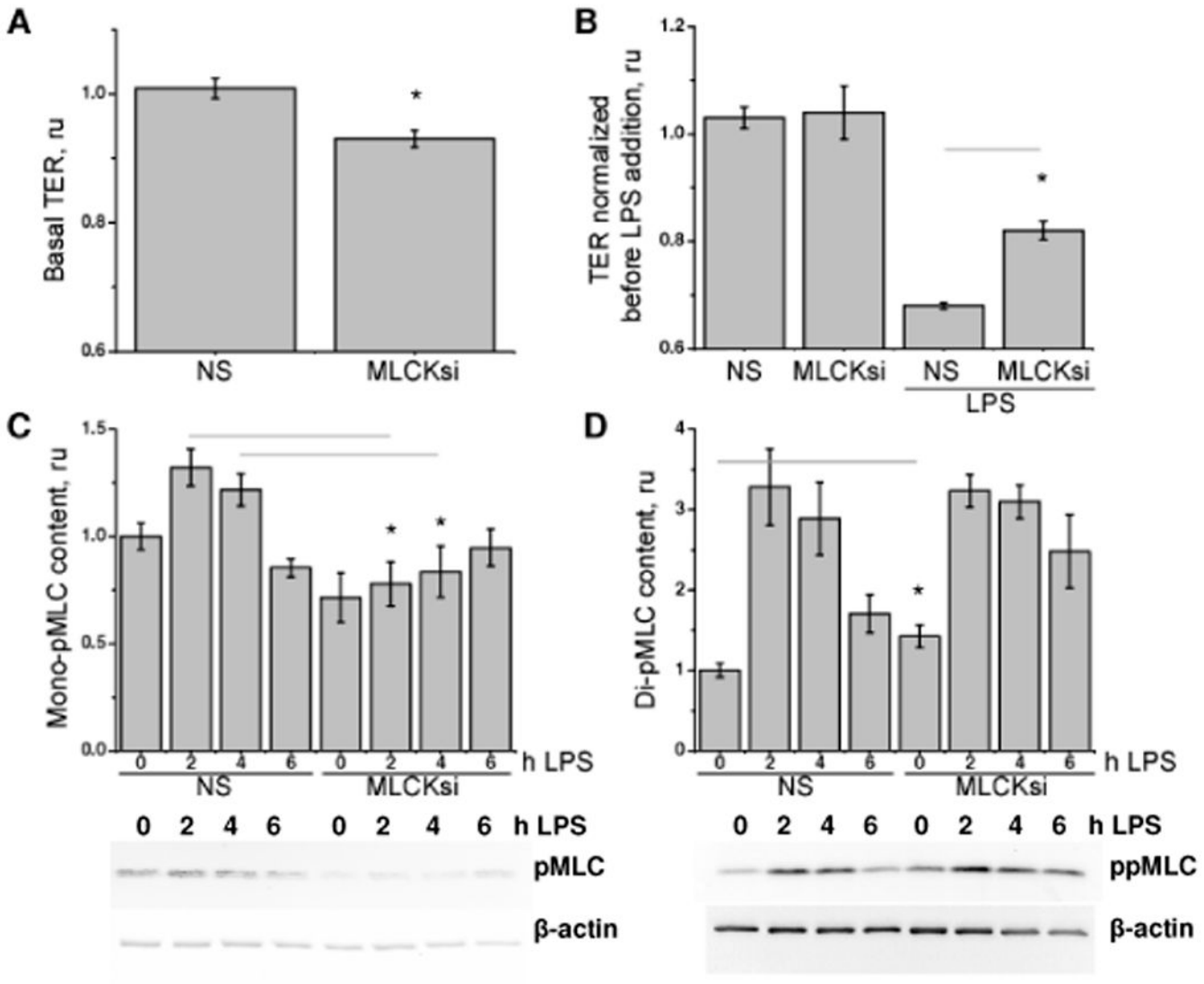

Fig. 4.

The effect of MLCK depletion on barrier permeability and MLC phosphorylation. A, B: HLMVEC grown on the gold electrodes were pretreated with 50nM MLCK siRNA (MLCKsi), or 50nM non-silencing RNA (NS). A: 48h later, TER was measured and normalized to the value of NS-pretreated monolayer. B: NS- and MLCKsi-pretreated monolayers were challenged by 100ng/ml LPS for 6h. TER values were normalized to the time point preceding LPS addition. C, D: HLMVEC grown in the wells of the 12-well plates were pretreated with NS and MLCKsi, then challenged with 100 ng/ml LPS for the time indicated, extracted and analyzed with anti-mono-(C) and anti-di-phospho-MLC (D) and anti-beta-actin (C,D) antibodies. Shown are representative blots (n=4) and histograms, analyzing variations in phospho-MLC band intensities (means±SE) expressed as folds of controls from NS-pretreated unchallenged cells (NS, 0h LPS). Values marked with * are significantly different ($p<0.05$) from the corresponding values in NS-treated group. For the normalization versus corresponding controls in each siRNA group, please refer to Fig 4 suppl. MLCK knock-down alleviates LPS-induced hyperpermeability and attenuates LPS-induced increase in MLC mono- and diphosphorylation.

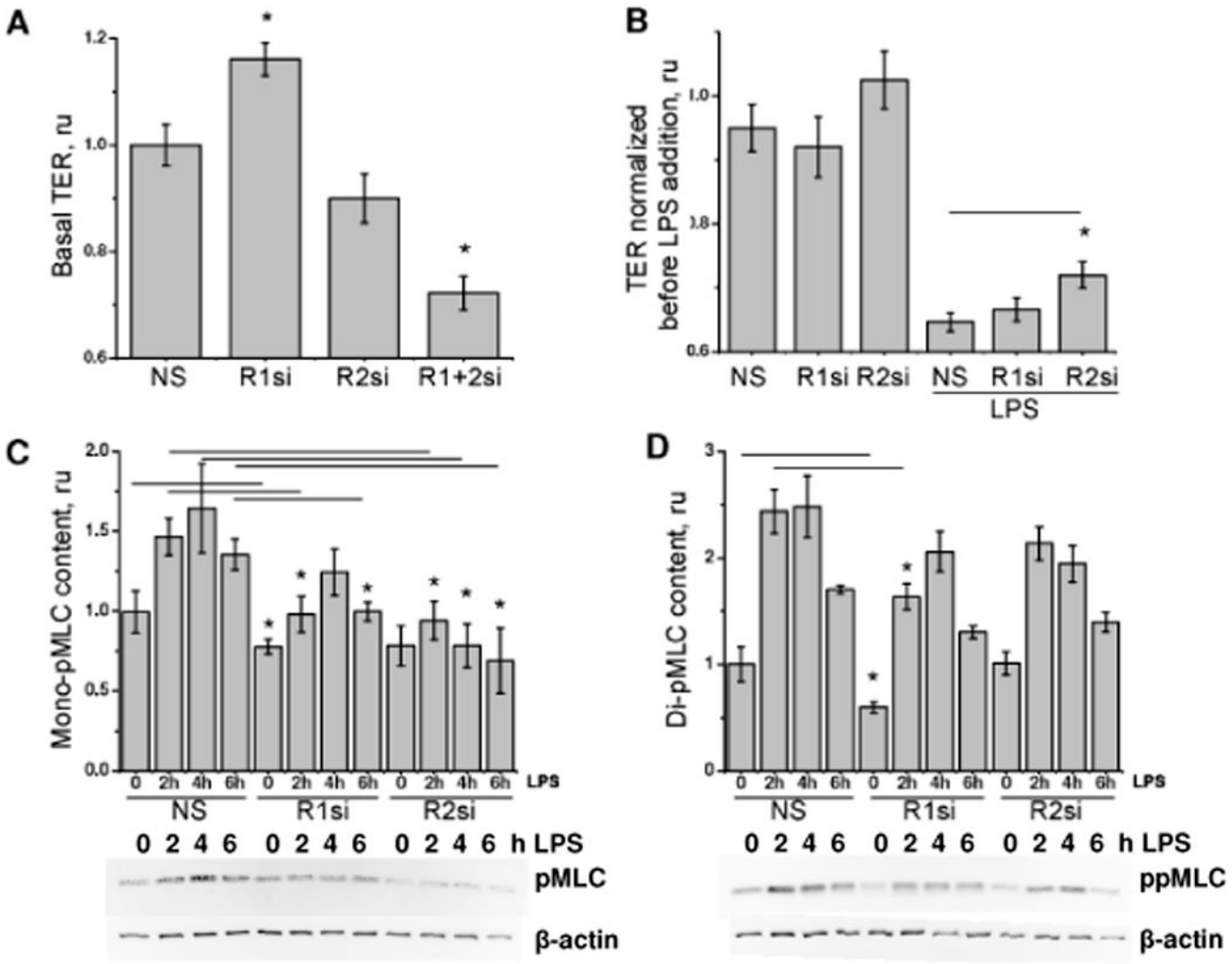

Fig. 5.

The effect of ROCK1/2 depletion on the barrier permeability and MLC phosphorylation. A: HLMVEC grown on the gold electrodes were pretreated with 50nM non-silencing RNA (NS), 50nM ROCK1 (R1si), 50nM ROCK2 (R2si) siRNA, or a combination of 25nM ROCK1 and 25nM ROCK2 (R1+2si). 48h later, TER was measured and normalized to the value of NS-treated monolayer. B: NS-, ROCK1 siRNA- and ROCK2 siRNA-pretreated monolayers were challenged with 100ng/ml LPS for 6h. TER values were normalized to the time point preceding LPS addition. C, D: HLMVEC grown in the wells of the 12-well plates were pretreated with NS, ROCK1- and ROCK2-specific siRNA, then challenged with 100 ng/ml LPS for the time indicated, extracted and analyzed with anti-mono-(C), anti-di-phospho-MLC (D) and anti-beta-actin (C,D) antibodies. Shown are representative blots (n=4) and histograms, analyzing variations in phospho-MLC band intensities (means±SE) expressed as folds of controls from NS-pretreated unchallenged cells (NS, 0h LPS). Values marked with * are significantly different ($p<0.05$) from the corresponding values in NS-treated group. For the normalization versus corresponding controls in each siRNA group, please refer to Fig 5 suppl. ROCK2 knock-down affects LPS-induced hyperpermeability and suppresses LPS-induced increase in MLC mono-phosphorylation.

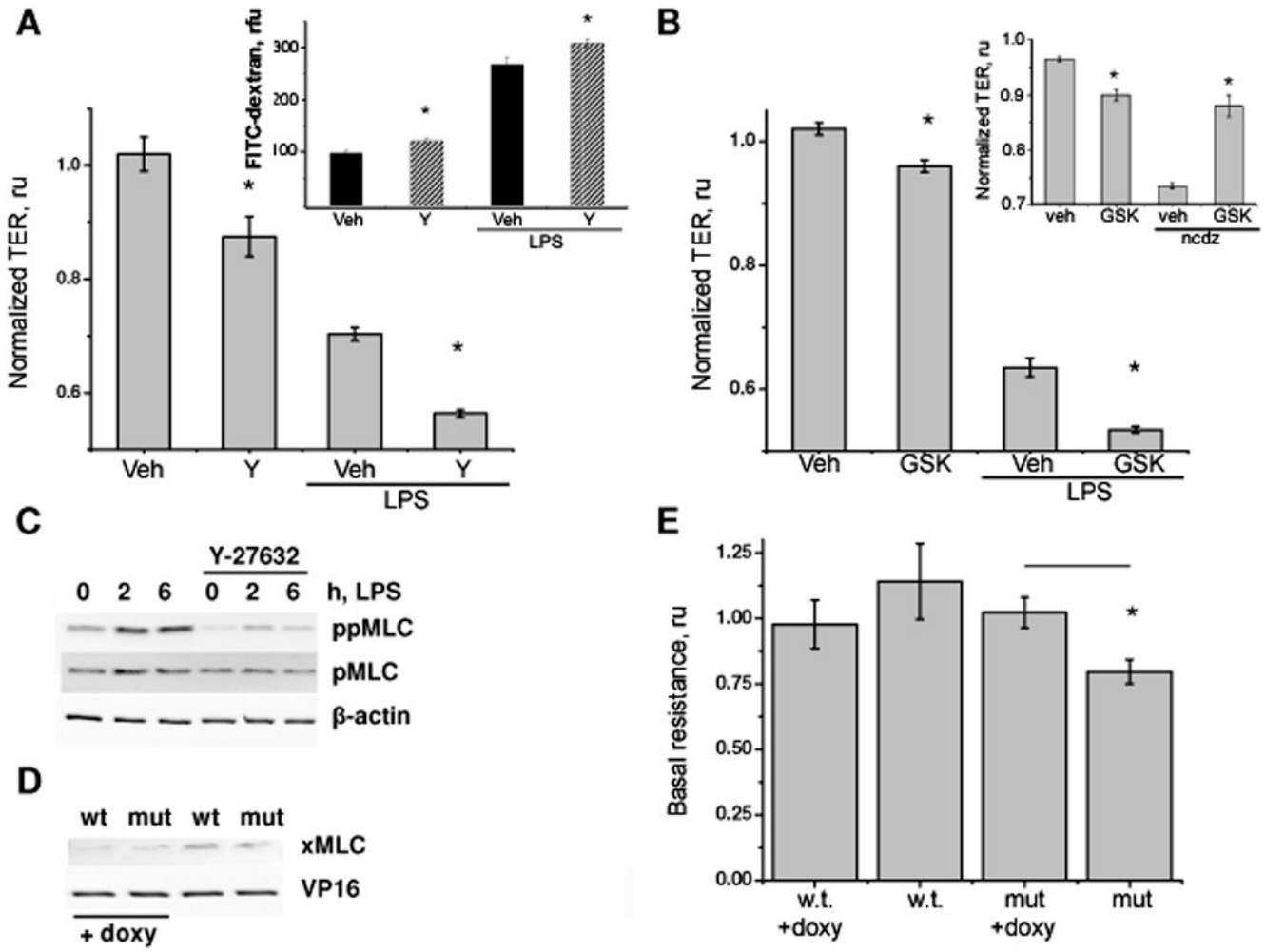

Fig. 6.

The effect of Rho-kinase inhibitors on the permeability of HLMVEC monolayers. A: Cells grown on the gold electrodes or the semi-permeable collagenated nylon membrane inserts (inset) were pre-treated with the vehicle control or 5μM Y-27632 for 15 min and then challenged with 100 ng/ml LPS for 6h. TER values were normalized to the time point preceding Y-27632 addition. FITC-dextran flux values were normalized to the permeability of the quiescent monolayers.. B: Cells grown on the gold electrodes were pre-treated with the vehicle control and 0.5μM GSK429286 for 15 min, then challenged with 7 ng/ml LPS for 6h or 0.5 μM nocodazole for 30 min (inset). TER values were normalized to the time point preceding GSK429286 addition. C: Cells grown in the wells of the 6-well plate were pretreated with the vehicle control or 5μM Y-27632 for 15 min and then challenged with 100 ng/ml LPS for the time indicated. Western blot analysis was done using mono- and di-phospho-MLC-specific antibodies and β-actin antibody as a loading control. D, E: Cells nucleofected with wild-type or mutant (T18AS19A) xMLC-expressing constructs were plated in the wells of 12-well plate or in the chambers with gold electrodes. Next day, cells were infected with Ad:tTA(VP16 tag); doxycycline was added to media where indicated. 48h after, cells were extracted and analyzed by Western Blot (D) or subjected to basal TER measurement (E). Western blot analysis was done using anti-xMLC antibody and anti-VP16 antibody. Shown are the means±SE of 3 (A, B) or 4 (E) parallel experiments. *indicate significant differences ($p<0.05$) with the corresponding controls. Inhibition of Rho kinases

in HLMVEC weakens basal and LPS-compromised endothelial barrier, while effectively suppressing MLC phosphorylation. Overexpression of MLC phosphorylation-deficient mutant decreases basal resistance across monolayer.

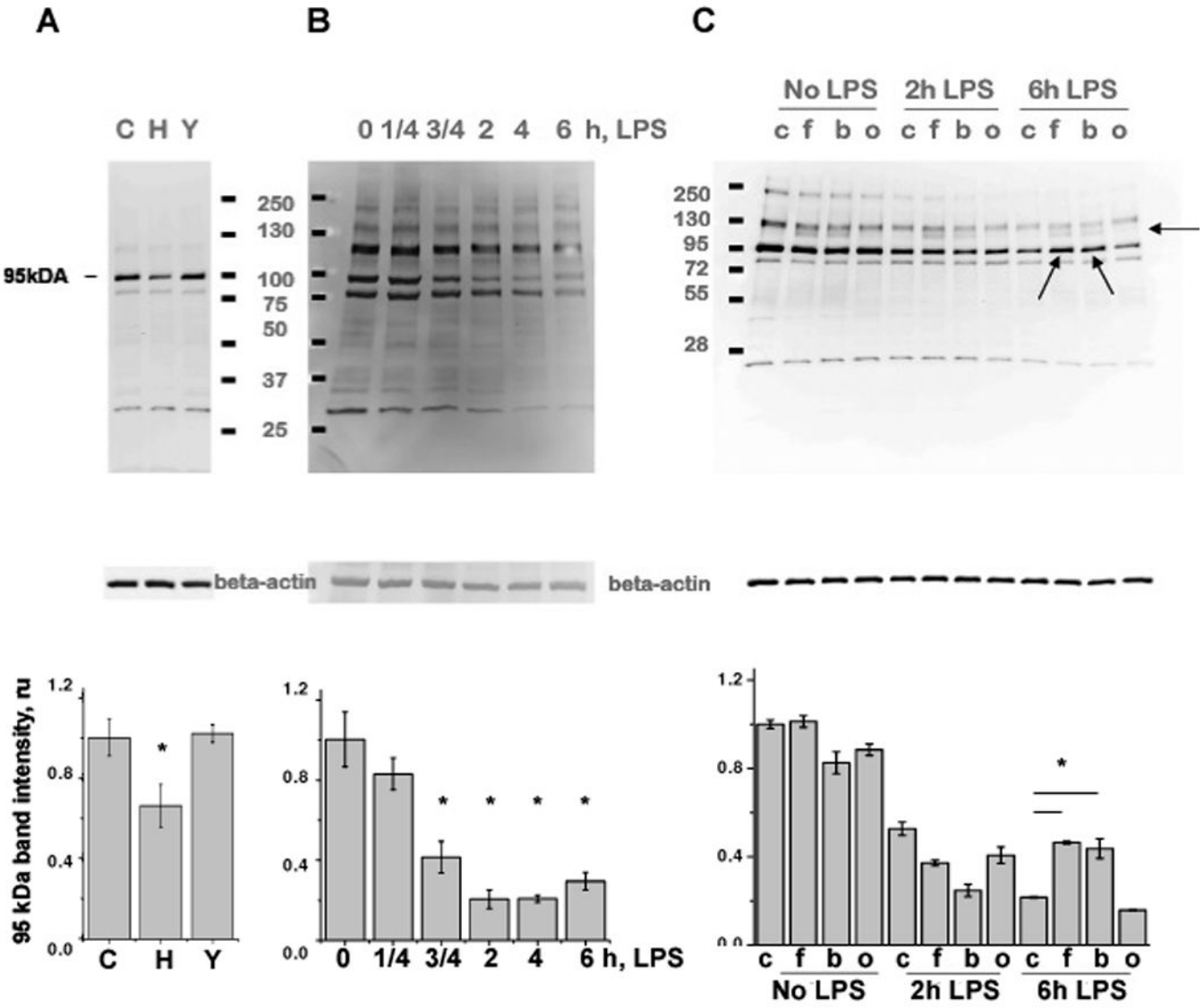

Fig. 7.

Modulation of PKA activity during the response to LPS. A: HLMVEC were pretreated with vehicle control (C), 10μM H-89 (H), or 5μM Y-27632 (Y), extracted and analyzed using antibody specific to the sites of PKA phosphorylation. β-actin staining was used a loading control. B: HLMVEC were challenged with 100ng/ml LPS for the time indicated, then analyzed as in (A). C: HLMVEC were pretreated with vehicle control (c), 5μM forskolin (f), 100μM bnz-cAMP (b), or 100μM o-me-cAMP (o), then challenged with 100ng/ml LPS for the time indicated and analyzed as in (A). Shown are the representative western blots out of 3 parallel experiments. A–C. The intensity of 95 kDa band was normalized to the loading control and presented as means±SE (n=3). * indicates significant differences ($p<0.05$) with the corresponding vehicle controls. LPS treatment leads to the overall weakening of the PKA phosphorylation-specific staining. Activation of PKA results in the appearance of a new phospho-band with MW of ~125 kDa (C, side arrow) and in the inhibition of the LPS-induced fading of the phospho-band with MW of ~ 95 kDa (C, arrows on the gel).

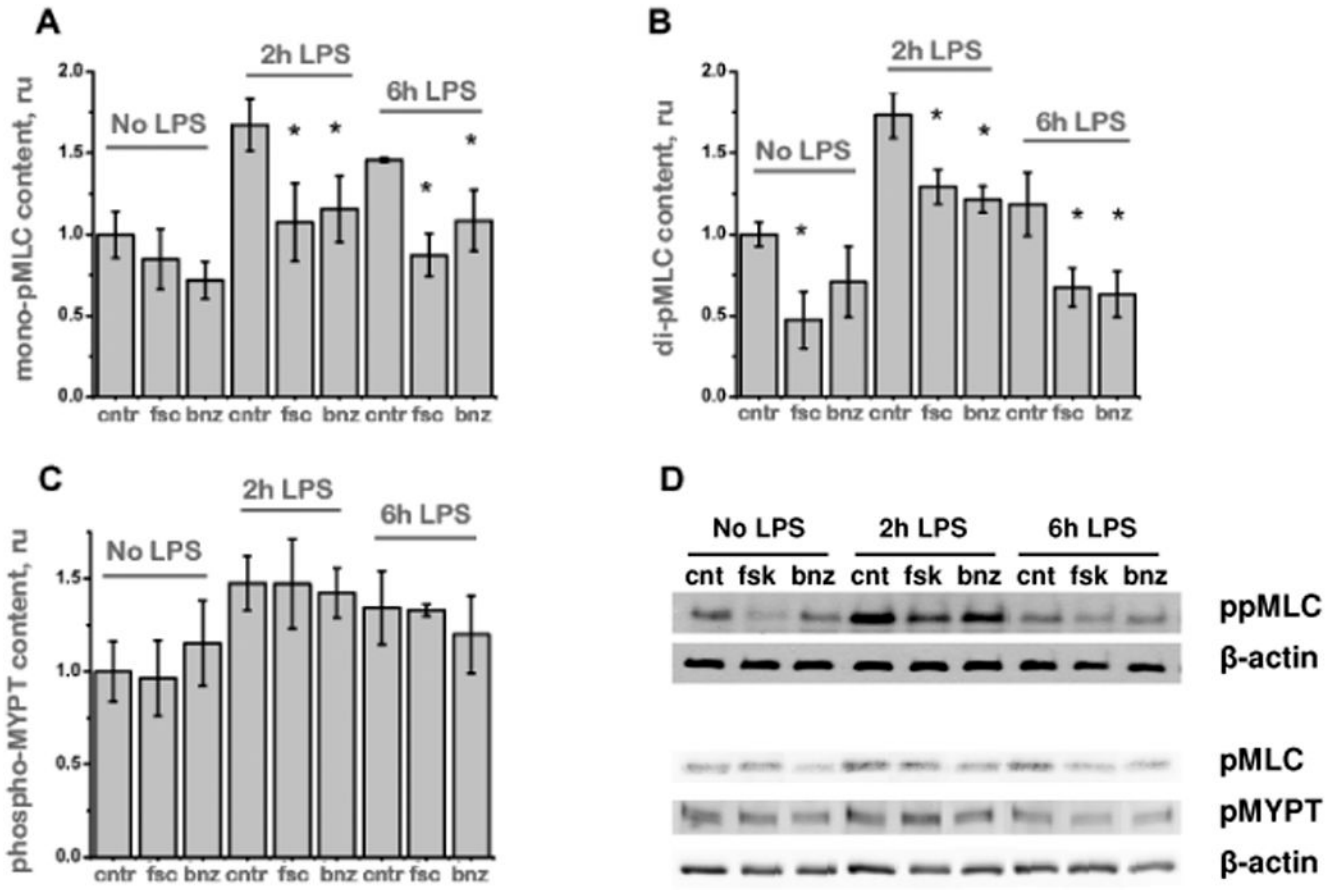

Fig. 8.

The effect of PKA activation on LPS-induced MLC and MYPT phosphorylation. HLMVEC grown in the wells of the 12-well plates were pretreated with the control vehicle, 5μM forskolin, or 100μM bnz-cAMP for 15 min, then challenged with 100 ng/ml LPS for the time indicated, extracted and analyzed with anti-mono-phospho-MLC (A, D), anti-diphospho-MLC (B, D), and anti-phospho-MYPT (C, D) antibodies. Phospho-band intensities were normalized to the intensity of β-actin staining. Shown are the means±SE (n=3). * indicates significant differences ($p<0.05$) with the corresponding vehicle control. Up-regulation of PKA activity significantly suppresses MLC phosphorylation in LPS-challenged cells, but this suppression is not achieved via the down-regulation of the ROCK/MYPT-dependent pathway.

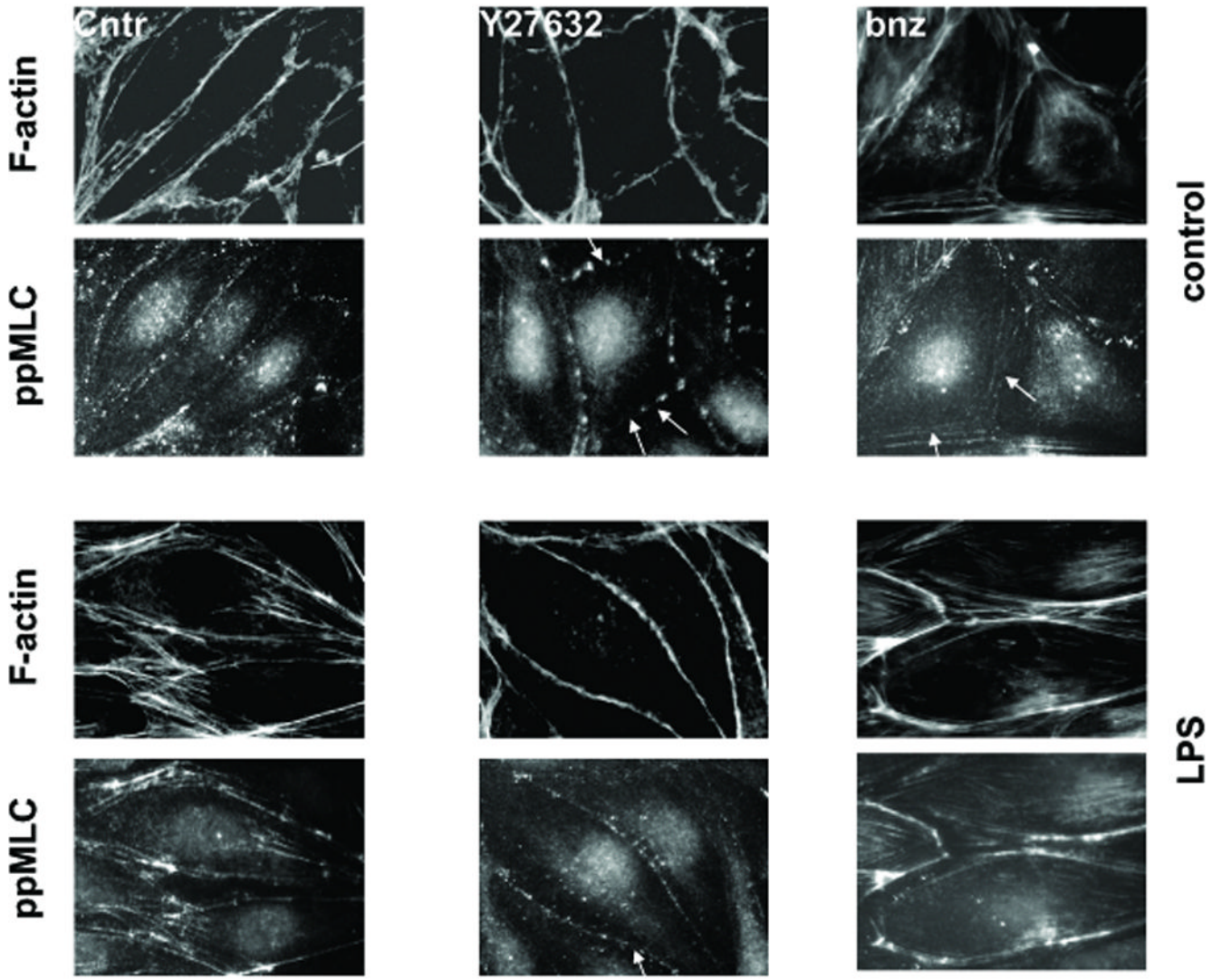

Fig. 9.

The effect of Rho kinase inhibitor Y-27632 and PKA activator bnz-cAMP on the LPS-induced rearrangement of the endothelial contractile machinery. Cells grown on collagen-covered coverslips were pretreated with vehicle control, 5μM Y-27632 or 100μM bnz-cAMP, then challenged with 100 ng/ml LPS for 2h, fixed, permeabilized, and probed with fluorescent phalloidin and anti-diphospho-MLC antibody. In unchallenged cells (upper panel), inhibition of ROCK diminishes di-phospho-MLC signal in the cortical actin area, whereas elevation of cAMP level increases this signal. LPS treatment (lower panel) induces moderate stress fiber formation concomitant with weakening of cortical structures. Inhibition of ROCK dramatically suppresses LPS-induced stress fiber formation, whereas elevation of cAMP fails to suppress this process.

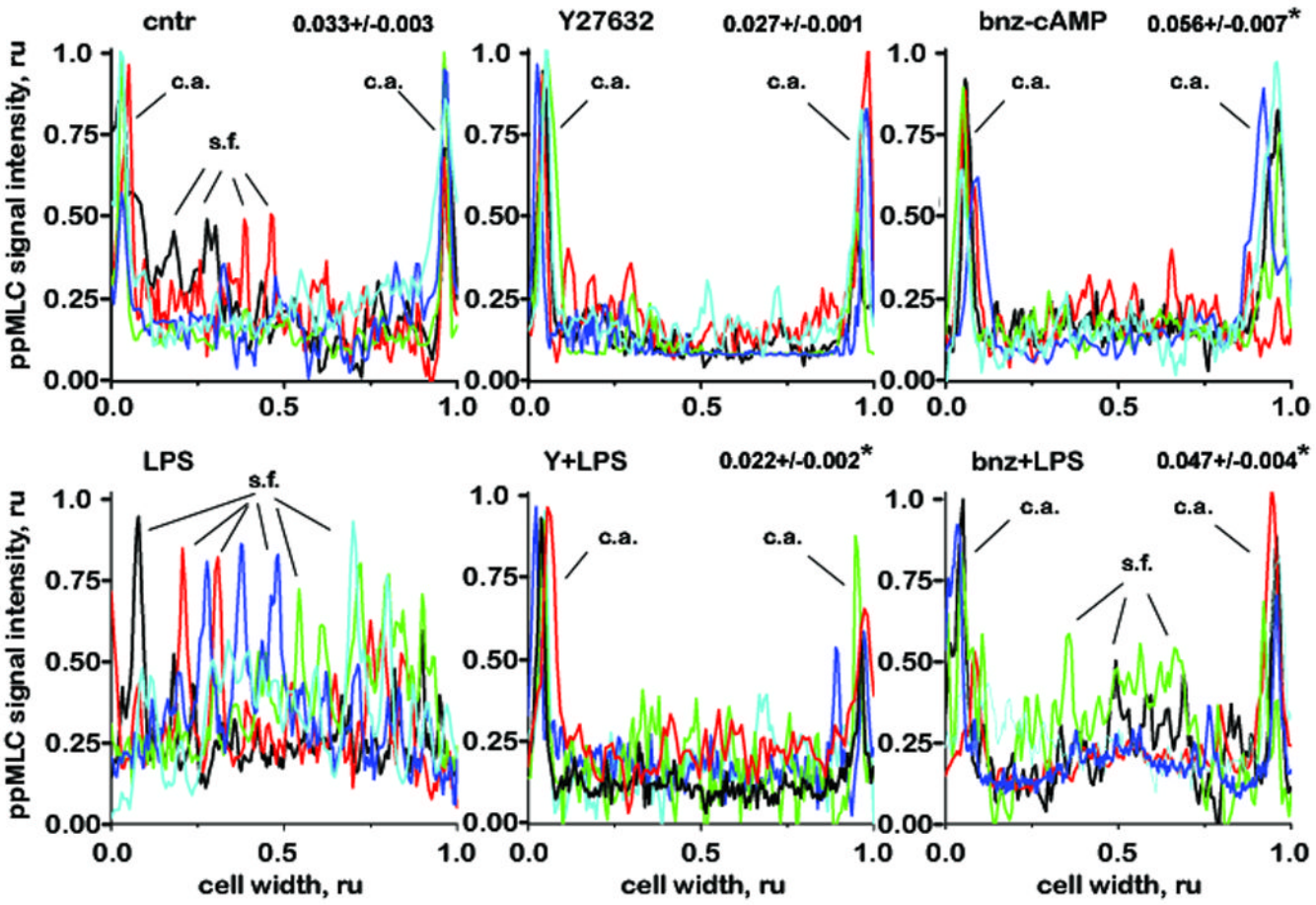

Fig. 10.

The effect of Rho kinase inhibitor Y-27632 and PKA activator bnz-cAMP on the LPS-induced redistribution of ppMLC in HLMVEC. The images obtained in the course of experiments on Fig. 9 were quantified as described in material and methods; and the profiles of the ppMLC distribution across the individual cells are depicted. The thickness of the cortical staining is presented as mean±SE (n=5) on the top of each graph. * indicates significant differences ($p<0.05$) with the control. The labels are: c.a.- cortical actin structures; s.f.- stress fibers. Un-challenged cells (upper panel) are characterized by the defined cortical ppMLC signal and some signal originated from cell-crossing stress fibers. In un-challenged cells, Y-27632 pretreatment does not significantly affect the thickness of the cortical structures, whereas bnz-cAMP pretreatment increases it. LPS treatment increases ppMLC signal derived from cell-crossing stress fibers and decreases peripheral ppMLC signal. In the presence of LPS, cortical structures of both Y-27632-pretreated and bnz-cAMP-pretreated cells exhibit lower thickness than in the absence of LPS; however, cortical structures of Y-27632/LPS-treated cells are thinner than those of control cells, whereas cortical structures of bnz-cAMP/LPS-treated cells are thicker than control structures.